Circuits and Systems
Mekelweg 4,
2628 CD Delft
The Netherlands
http://ens.ewi.tudelft.nl/

CAS-2009-MS-07

M.Sc. Thesis

Human Movement Characterization in Indoor Environment using GNU Radio Based Radar

Bruhtesfa E. Godana

Abstract

Human activity characterization based on gait signatures is important in several applications including medical, elderly care, police, biometric identification, etc. Cameras and on-body accelerometers are widely investigated for characterizing human activity. Nonetheless, in order to achieve wide acceptance, sensors to be used for these applications should be unobtrusive and people's privacy should be respected. Radar is a promising technology for human activity characterization as it satisfies these requirements and operates largely unaffected by environmental conditions and the presence of blocking objects. This thesis presents algorithms for radar signal processing and human activity quantification, identification and classification in indoor environment. Methods to extract parameters of human motion such as activity level, displacement, velocity, step length, velocity bandwidth, etc., from radar data are suggested and discussed. The developed algorithms are evaluated in an experimental low-cost radar prototype using Universal Software Radio Peripheral and GNU Radio.

TU Delft

Faculty of Electrical Engineering, Mathematics and Computer Science — Delft University of Technology

Human Movement Characterization in Indoor Environment using GNU Radio Based Radar

Thesis

submitted in partial fulfillment of the
requirements for the degree of

Master of Science

in

Electrical Engineering

by

Bruhtesfa E. Godana
born in Dessie, Ethiopia

This work was performed in:

Circuits and Systems Group
Department of Telecommunications
Faculty of Electrical Engineering, Mathematics and Computer Science
Delft University of Technology

Delft University of Technology

Delft University of Technology
Department of
Telecommunications

The undersigned hereby certify that they have read and recommend to the Faculty of Electrical Engineering, Mathematics and Computer Science for acceptance a thesis entitled **"Human Movement Characterization in Indoor Environment using GNU Radio Based Radar"** by **Bruhtesfa E. Godana** in partial fulfillment of the requirements for the degree of **Master of Science**.

Dated: June 19, 2009

Chairman:

Prof.dr.ir. Alle-Jan Van der Veen

Advisors:

Dr. Geert Leus

Dr. Andre Barroso

Committee Members:

Prof.dr. O. Yarovoy

Abstract

Human activity characterization based on gait signatures is important in several applications including medical, elderly care, police, biometric identification, etc. Cameras and on-body accelerometers are widely investigated for characterizing human activity. Nonetheless, in order to achieve wide acceptance, sensors to be used for these applications should be unobtrusive and people's privacy should be respected. Radar is a promising technology for human activity characterization as it satisfies these requirements and operates largely unaffected by environmental conditions and the presence of blocking objects. This thesis presents algorithms for radar signal processing and human activity quantification, identification and classification in indoor environment. Methods to extract parameters of human motion such as activity level, displacement, velocity, step length, velocity bandwidth, etc., from radar data are suggested and discussed. The developed algorithms are evaluated in an experimental low-cost radar prototype using Universal Software Radio Peripheral and GNU Radio.

Acknowledgments

I would like to express my heartfelt thanks to a number of people, without whom this thesis work would not have been accomplished. First and foremost, I would like to thank my advisors Dr. Andre Barroso and Dr. Geert Leus for their supervision, guidance and encouragement. Andre has not only supervised my work; he has also inspired, encouraged and showed me the passion in scientific research. I have learnt and benefited a lot from him. Geert has helped me a lot guiding me with his nice ideas and suggestions at each step of the work and correcting the thesis finally. I would like to thank him for his dedication, encouraging attitude and for being always there to help me out.

I would also like to thank my colleague A.Dharamshi for working close with me and helping me while making experiments. My thanks also goes to the Distributed sensor systems group in Philips Research, Eindhoven. I would like to mention specially Mr. Peter Rutten for helping me by providing equipments and working space in the lab.

Last but not least, I would like to thank my Family and Aida M. for their love, support and encouragement. I thank Aidy so much for her incredible love and passion. I am also grateful to my friends Anteneh and Getachew for the nice time together and for their brotherly advices.

Bruhtesfa E. Godana
Delft, The Netherlands
June 19, 2009

Contents

1 Introduction **1**
- 1.1 Movement Monitoring Applications . . . 1
- 1.2 Advantages and Limitations of Radar for Human Activity Monitoring . . . 3
- 1.3 Related Work . . . 4
- 1.4 Thesis Goals . . . 5
- 1.5 Thesis Organization . . . 5

2 Human Movement Characterization **6**
- 2.1 Human Movement Model . . . 6
  - 2.1.1 Velocity Profile . . . 6
  - 2.1.2 Radar Cross Section (RCS) . . . 8
- 2.2 Methods to characterize human motion . . . 8
  - 2.2.1 Human Movement Identification . . . 9
  - 2.2.2 Human Activity Classification . . . 10

3 Doppler Shift in Indoor Environment **11**
- 3.1 Doppler Effect in Radars . . . 11
  - 3.1.1 Principle of Doppler Shift . . . 11
  - 3.1.2 Doppler Shift and Radar Configurations . . . 13
  - 3.1.3 Clutter in an indoor Environment . . . 14
  - 3.1.4 Doppler Shift in Multipath Environment . . . 14
- 3.2 Radar Equation and SNR . . . 16
- 3.3 Requirements for Human Movement Characterization . . . 19
- 3.4 Radar Types . . . 20
  - 3.4.1 Unmodulated Continuous Wave (CW) Radar . . . 21
  - 3.4.2 Pulse Doppler Radar . . . 21
  - 3.4.3 Pseudo-random sequence (PRS) Radar . . . 22

4 Time-Frequency Estimation **24**
- 4.1 Signal pre-Processing . . . 24
  - 4.1.1 I/Q Imbalance Correction . . . 25
  - 4.1.2 FIR Filtering and Decimation . . . 25
- 4.2 Non-Parametric Frequency Estimation . . . 26

4.3 Parametric Frequency Estimation . . . 27
4.3.1 Signal Model . . . 27
4.3.2 MUSIC . . . 28
4.3.3 ESPRIT . . . 29
4.4 Joint Time-Frequency Processing . . . 29
4.4.1 Short time Fourier transform (STFT) . . . 30
4.4.2 Spectrogram . . . 32
4.4.3 Sliding Window Parametric Estimators . . . 32
4.5 Background Spectrum Subtraction . . . 34
4.6 Quadrature Demodulation . . . 36

5 Parameter Extraction **38**
5.1 Parameters to Quantify Activity . . . 38
5.1.1 Activity Index . . . 38
5.1.2 Displacement versus Time . . . 39
5.1.3 Direction of Motion . . . 40
5.2 Identification Parameters . . . 40
5.3 Classification Parameters . . . 41
5.4 Velocity Profile . . . 42

6 The Experimental Platform **44**
6.1 Software Defined Radio . . . 44
6.2 Platform Overall Architecture . . . 45
6.3 Limitations of the Experimental Platform . . . 46
6.3.1 Isolation in the USRP . . . 46
6.3.2 Phase Noise & Frequency offset . . . 47
6.3.3 Maximum Distance . . . 48
6.3.4 Maximum Bandwidth . . . 48
6.4 Radar Types and Parameters . . . 49
6.4.1 The Experimental Platform for Different Radar Types . . . 49
6.4.2 Choice of Parameters . . . 49
6.5 Advantages of GNU Radio based Radar . . . 50
6.5.1 Low Cost . . . 50
6.5.2 Flexibility . . . 51

7 Evaluation & Discussion **52**
7.1 Experimental Setup . . . 52
7.2 Human Activity Quantification . . . 53
7.2.1 Activity Index . . . 53
7.2.2 Displacement versus Time . . . 54
7.2.3 Direction of motion . . . 56
7.3 Human Movement Identification . . . 57
7.3.1 Received Signal . . . 57
7.3.2 Spectrograms . . . 58

7.3.3 Torso Velocity . . . 60
7.3.4 Cadence Frequency . . . 61
7.4 Human Activity Classification . . . 62
7.4.1 Spectrograms . . . 63
7.4.2 Torso Velocity . . . 64
7.4.3 Step Length . . . 65
7.4.4 Velocity Bandwidth . . . 65
7.4.5 Standard Deviation . . . 67
7.5 Velocity Profile . . . 67
7.6 Conclusion . . . 68

8 Conclusions & Future Work **69**
8.1 Conclusion . . . 69
8.2 Future Work . . . 70

A Universal Software Radio Peripheral **75**
A.1 The USRP . . . 75
A.2 Daughter boards . . . 78

B GNU Radio **81**
B.1 Introduction . . . 81
B.2 Blocks & Signal Flow Graphs . . . 82
B.3 Radar Signal Flow Graphs . . . 82

List of Figures

2.1 Human movement velocity profile [7] 7

3.1 Movement of a person and Doppler radar 12
3.2 Doppler Effect in a multipath environment 16
3.3 Ratio of reflected to direct signal 19

4.1 Cascaded decimation stage and FIR filter frequency response 26
4.2 Hamming Window 31
4.3 Background signal spectrum 34
4.4 Spectrogram before and after background subtraction 36

6.1 GNU Radio based Radar Block Diagram 46
6.2 Frequency offset and Phase noise in the received signal 47

7.1 Experimental Setup 53
7.2 Power Variation 53
7.3 Activity Index 54
7.4 Experiment-2 54
7.5 Displacement versus time 55
7.6 Experiment-3 55
7.7 Displacement from sawtooth motion 56
7.8 Direction of motion 57
7.9 Experiment-4 57
7.10 Time domain signal 58
7.11 STFT based Spectrogram Estimation 59
7.12 MUSIC based Spectrogram estimation 59
7.13 Torso velocity Estimations 61
7.14 Doppler vs cadence frequency 61
7.15 Cadence frequency 62
7.16 Spectrograms from different Activities 63
7.17 MUSIC spectrograms for walking and jogging 64
7.18 Classification based on torso velocity 64
7.19 Cadence frequency of the gait 65
7.20 Classification based on velocity envelopes 66

7.21 Standard deviation of power within velocity bandwidth 67
7.22 Velocity Profile using local maxima in MUSIC 68

A.1 The USRP with basic transmit and receiver Daughter boards 76
A.2 USRP motherboard 76
A.3 Digital Up converter in USRP 77
A.4 Digital down converter section in USRP 78
A.5 PLL based frequency multiplier 80

B.1 SDR structure using GNU radio and USRP 83

Nomenclature

ADC Analog to Digital Converter

AI Activity Index

BPSK Binary Phase Shift Keying

CIC Cascaded Integrate Comb

CW Continuous Wave

DAC Digital to Analog Converter

DDC Digital Down Converter

DFT Discrete Fourier Transform

DUC Digital Up Converter

ESPRIT EStimation of Signal Parameters using Rotational Invariance Technique

FFT Fast Fourier Transform

FIR Finite Impulse Response

FPGA Field Programmable Gate Arrays

HBF Half Band Filter

MUSIC MUltiple SIgnal Classification

PGA Programmable Gain Controller

PLL Phase Locked Loop

PRF Pulse Repetition Frequency

PRS Pseudo Random Sequence

RCS Radar Cross Section

RF Radio Frequency

Rx Receiver

SDR Software Defined Radio

SNR Signal to Noise Ratio

STFT Short Time Fourier Transform

Tx Transmitter

USRP Universal Software Radio Pheripherial

VCO Voltage Controlled Oscillator

XCVR Daughterboard used as RF frontend

Chapter 1

Introduction

Characterization of human movement is very important in diversified fields including medical, elderly care, police, security and law enforcement, biometric identification, etc. There is a vast research on developing an accurate model for different human activities. The major goal of this research is to come up with parameters that can be used to characterize human activity remotely using an appropriate sensor. One of these sensors is radar. Radar makes remote characterization of human activity possible by using the Doppler effect of electromagnetic waves. The major advantages of radar with respect to other technologies are the fact that it allows unobtrusive monitoring and works unaffected by environmental conditions.

1.1 Movement Monitoring Applications

Characterization of human movement includes human activity quantification, identification and classification (in the context of this thesis). **Quantifying** activity involves calculating an index proportional to the level of the movement, the so called activity index (AI). Radars associated with human movement are commonly presence detection radars that provide just binary information of whether or not there is motion. In contrast to this binary information, quantification means providing an output that is proportional to the level of movement. The level of activity actually depends on the type of movement, the number of people, the presence of other moving objects, etc.; however, the goal of the quantification is to come up with an index that quantifies indoor activity without taking these factors into consideration. **Identification** of human movement on the other hand involves identifying whether the activity index computed is due to movement of a person or not. Other movements in an indoor environment such as rotation of a fan, movement of pets, etc., can lead to a wrong estimate of the level of activity. So, identification involves discriminating human movement from non-human movements. **Classification** goes a bit farther; it involves identifying what type of movement the person is making. An activity index can show the level of activity in a room; however, it does not tell whether the person is sitting, walking or jogging for instance. So, human activity classification means to come up with a possible match to an activity that is being done from

a list of possible activities.

The characterization of human activity in an indoor environment is useful in many sectors including medical centers, care takers, police, etc. In the medical sector, remote patient activity monitoring saves time and energy for doctors. The wellness of patients can be related to the level and type of activity. For instance, the rehabilitation status of operated patients can be related to the level of movement. Police may be looking for suspects hidden behind or in a building; thus, monitoring their activity remotely without violating privacy will be essential. Elderly care is also an important application of human movement characterization. There are a lot of elderly people living alone in their home or in elderly care centers nowadays. One of the parameters that can be related to the health, emotion and wellness of these elderly people is their movement pattern. Moreover, fall detection which is an important part of elderly care can also be identified from the pattern of movement. Nowadays, there is also research going on to use a person's movement pattern for biometric identification as the movement pattern of each person is said to be unique enough for identification. All these applications show that remote characterization of a movement pattern has very important applications. However, most of these applications require a sensor that enables to monitor movement remotely in unobtrusive way and without violating privacy.

There are many sensors based on different technologies for presence detection and activity quantification. However, the information from most of these sensors is limited. In addition, some of these sensors can easily be blocked by obstacles or walls. Sensors like the accelerometer[1] have to be attached on the body which makes them inconvenient for most people. Networking these on-body sensors and transmitting information wirelessly to a fixed node is another problem. Radar is a promising technology for human movement monitoring that avoids most of these problems. Radar is less privacy-violative as compared to other sensors, can be mounted unobtrusively and allows monitoring through the wall. Moreover, the fact that radar is not largely affected by lighting and weather conditions makes it an attractive technology for remote movement monitoring.

Radar measures the Doppler shift of electromagnetic waves in order to characterize movement. However, most of the commercial Doppler radars that exist nowadays are specifically designed for measuring velocity of a rigid object that moves at a constant, high velocity such as a car or airplane. Therefore, these radars can neither be directly used nor adapted for measuring time varying movement patterns of human beings in real time. Therefore, a flexible radar prototype should be designed by taking into consideration the basic components of radar. The software of this prototype should be open source, easily controllable and flexible to implement the required algorithms. Software defined radio (SDR)[2] based radars gives the flexibility to implement different type of radars and the corresponding signal processing algorithms using the same basic hardware. Moreover, new signal processing algorithms can be easily integrated into already existing software blocks for real time operation.

[1] An accelerometer is a sensor which computes the level of activity from acceleration measurements.

[2] Software defined radio is a radio communication system where signal modulators and demodulators are implemented in software on a personal computer or embedded processors.

1.2 Advantages and Limitations of Radar for Human Activity Monitoring

Nowadays, there are many sensors widely used for automated human activity monitoring and detection. Cameras are the most common ones. Processing a sequence of images from cameras is being used for human activity characterization. Accelerometers and other similar sensors are used for activity level detection. Infrared presence detectors which measure change in heat or infrared energy are common nowadays for automatic lighting control. Radar has in general the following advantages with respect to these and other similar sensors:

- ***Less privacy-violative***: Unlike cameras which shows images of the activities that the human target is doing; radar monitors only limited information of the target such as position and velocity.
- ***Non-obstructive observation***: Radar has longer operation distance and can penetrate non-metallic objects, which is important for through-the-wall detection. Radio waves are also not obscured by clothing; for instance, radar can be used for concealed weapon detection.
- ***Insensitive to environmental effects***: Radar is not largely affected by light and weather conditions which significantly affect other sensors.
- ***Unobtrusive***: Radar can be mounted invisibly behind a wall[3] or in ceiling.
- ***More information***: Unlike other sensors, radar gives more information about the target such as velocity, direction of motion and distance in addition to presence detection.

However, a radar sensor has also limitations and disadvantages compared to other sensors. These include:

- ***Extensive signal processing***: Obtaining useful information from a radar system is challenging and requires extensive signal processing.
- ***Blind to tangential motion***: Radar measures only the radial motion of a target.
- ***More hardware***: A radar system contains more complex hardware than these systems. In addition, radar with an antenna array or more than one radar (distributed radars) may be required to track a human target in presence of multi-movers.
- ***Power and frequency Regulation***: Radars should obey the tight power and frequency regulations in the radio spectrum.
- ***Health Risk***: It is confirmed that excessive radio waves cause health risk to the body [28]. Thus, the other limitation of a human activity monitoring radar is that the power must be kept below the safety limit.

[3] This holds true for non-metallic walls only and depends on other factors too.

1.3 Related Work

A lot of literature has been revised on different approaches and technologies for human being detection and ranging. This section reviews the major literature available on radars for human being identification and classification. Human activity characterization using various radar types has been studied in various literature. The use of wideband noise radar sensors for human detection is described in [1]. Detection of human beings and ranging using ultra-wideband noise sensors is also described in [2]. The author of [3] uses multiple frequency continuous wave radar for classifying humans, animals and vehicles and for ranging.

Human gait[4] analysis using continuous wave (CW) radars is also studied in some literature. Otero [4], uses a 10GHz CW radar using micro-patch antennas to collect data and to attempt classifications, including male and female. A simulation based gender discrimination using the spectrogram is also discussed in [5]. The authors of [6] use a 24GHz CW radar to obtain velocity information. In another paper, [7] the same authors use again data from their radar to attempt to classify between a human and a non-human object. Artificial neural networks for classifying human activities based on micro-Doppler signatures[5] are also shown in [8].

All the papers listed above use fast Fourier transform based frequency estimation. There is also some research on using other transforms. The authors of [9] tried to introduce the chirplet transform as an analysis tool, but they did not come up with its meaning in the gait analysis. The Hilbert-Haung Transform for non-linear and non-stationary signals in wide band noise radars is also suggested in [10] by the authors of [2]. A complex but more accurate iterative way to obtain each pixel in the spectrogram in a bid to improve the frequency resolution and side lobes of the fast Fourier transform is also discussed in [11].

Both the model based and experimental research above assumes that there is a single mover only. There is also research done on using Doppler based direction of arrival sensing. The PhD dissertation, [12] describes in detail how to design a pulse Doppler radar using an antenna array and the way to come up even with 3-D tracking. The authors of [13] and [14], also describe ways to track humans using Doppler information and antenna arrays.

The use of universal software radio peripheral (USRP)[6] as passive radar has been introduced by Mr. Eric Blossom[7]. Using a USRP as active radar has not yet been explored. However, the author of [27] has written a thesis on using a USRP as a pulse Doppler radar for airplane detection by adding some hardware modification.

[4]Gait is the pattern of human movement or locomotion.

[5]A micro-Doppler signature is the small scale pattern of motion obtained as a result of the Doppler phenomenon.

[6]The universal software radio peripheral is a general purpose transceiver that allows to create a software radio using a computer with a USB2 connection.

[7]Eric Blossom is the founder and overall architect of the GNU Radio project.

1.4 Thesis Goals

The major goal of the thesis is to extract human movement parameters that can be used for quantifying, identifying and classifying human movement, in particular walking, in an indoor environment using a low cost radar sensor.

Strategies to identify, quantify and classify human movement using continuous wave (CW) Doppler radar are investigated. Signal processing algorithms are designed and implemented to extract human movement parameters that are employed by these strategies. A low-cost radar platform, that uses a USRP as hardware and GNU Radio[8] as software, is designed and implemented in order to obtain experimental human movement data. The algorithms suggested for human movement characterization are then evaluated by obtaining human movement parameters such as activity index, velocity, stride length, etc., from a data obtained by pre-defined experiments.

1.5 Thesis Organization

The thesis is organized as follows. The second chapter revises the velocity profile and radar cross section (RCS) of human body according to available human movement models. The velocity profile is used to discuss human movement parameters that can be used for identification and classification of human activity. In Chapter 3, general expressions for the Doppler signal received in a multipath environment and the expected signal to noise ratio (SNR) are derived and discussed in different scenarios. Chapter 4, discusses time-frequency estimation techniques and the corresponding parameters used to obtain a useful Doppler representation of the motion: the spectrogram. The Doppler signal model in Chapter 3 is also utilized to estimate the signal spectrum using high resolution spectral estimators. In Chapter 5, different methods to extract parameters of human movement for activity quantification, identification and classification are discussed. Most of these parameters are extracted from the spectrogram estimated in Chapter 4. Chapter 6 describes a low-cost software defined platform that is used as a continuous wave radar in this thesis. The overall architecture and limitations of the platform are described. The Chapter concludes discussing the choice of parameters and advantages of such a flexible platform. Then, the parameter extraction algorithms are evaluated and justified in Chapter 7 based on pre-defined experiments. Finally, the major points drawn from the thesis are summarized based on the results and further work which can make the Doppler estimation more informative is suggested.

[8] GNU Radio is a free software toolkit for designing and implementing software defined radio systems.

Chapter 2

Human Movement Characterization

In this Chapter, the basic principle of a widely used human movement model is introduced. Velocity profile and RCS are discussed as the important parameters that describe a human locomotion model. The next section makes use of the human movement model and talks about parameters which can be extracted from the model for human movement identification and classification purpose. These parameters have a unique value for human motion which helps in identification and differ from activity to activity which can be used in classification.

Researchers that study human locomotion commonly use the following terminology for two major parts of the body: torso and appendages. **Torso** refers to the main part (trunk) of the body and **appendages** refer to the other parts of the body, particularly it refers to the oscillating hands and legs.

2.1 Human Movement Model

The human movement model is the starting point for human activity characterization. After studying the relationship between the different parts of the body during locomotion; parameters that make the locomotion distinct can be identified. The most important human gait parameters that make human motion unique in radar based activity monitoring are velocity profile and RCS. A velocity profile and RCS can be defined for each of the major parts of the human body.

2.1.1 Velocity Profile

The velocity profile refers to the relative velocities that the different parts of the human body attain during locomotion, in other words it is the velocity versus time pattern of the parts of the body during movement. There is vast research on human movement modeling; however, almost all of the models rely on dividing the non-rigid human body into the most significant 12 rigid body parts and modeling the velocity profile and RCS of these rigid components. One of the most common human movement models, [15] decomposes the body into 12 parts consisting of the torso, lower and upper part of each

leg, lower and upper part of each arm, the head and each of the right and left foot. This model tries to come up with kinematics of each of these body parts. Another known model was developed by Troje, [16] which is based on 3-D position analysis of reflective markers worn on the body using high resolution camera. Based on the analysis of the experiments, Troje says that the velocity profile of each body part can be represented using low order Fourier series. This is described as follows.

Assume a person moving at a constant velocity, V with respect to an initial point in a certain direction. Let's say we divide the body into M rigid body parts. Each of the body parts including the torso have a velocity profile, $v_m(t)$ that can be represented as a sum of sinusoids which can be given by:

$$\begin{aligned} v_m(t) &= V + A \cdot \{k_{m1} \cdot \sin(\omega_c t + p_m) + k_{m2} \cdot \cos(\omega_c t + p_m) + \\ &\quad k_{m3} \cdot \sin(2\omega_c t + p_m) + k_{m4} \cdot \cos(2\omega_c t + p_m)\} \end{aligned} \tag{2.1}$$

where, $k_{m1}, ..., k_{m4}$ and $p_m\{0 \leq p_m \leq \pi\}$ are constants that characterize each of the body parts. The values of $k_{m1}, ..., k_{m4}$ is largest for the legs and smallest for the torso. The phase, p_m shows the locomotion mechanism of the body; for instance, the right leg and left arm combination move 180^o out of phase with respect to the left leg and right arm. A is a constant that has a specific value for the different human activities like walking, running, etc. The cadence frequency, ω_c is the rate of oscillation of the body and it is related to the velocity of the person as $f_c = B \cdot \sqrt{V}$, where B is a constant and depends on the type of motion.

A simulation of the velocity profile based on this model is shown in Figure 2.1.

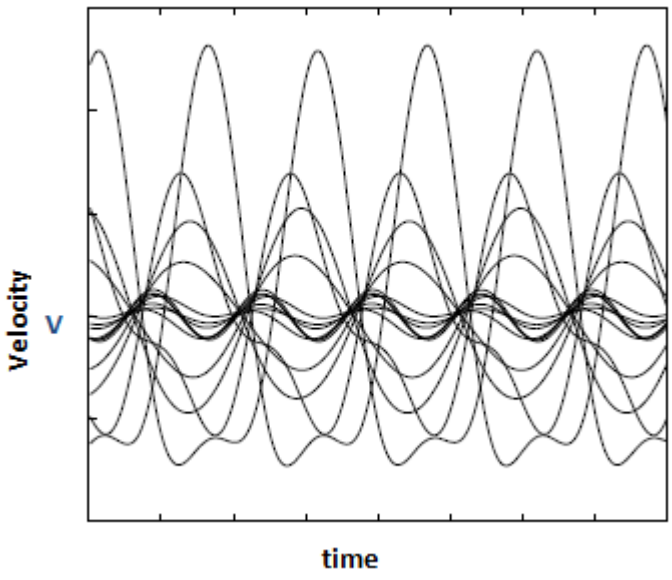

Figure 2.1: Human movement velocity profile [7]

The figure shows the velocity trajectory of each body part as a function of time. It shows that the amplitude of oscillation of each body part is different. However, as shown by (2.1), all the body parts oscillate at the same frequency ω_c and its second harmonic.

2.1.2 Radar Cross Section (RCS)

The RCS, σ is a parameter that describes a target's ability to reflect radar signals in the direction of the receiver. It is defined as 4π times the ratio of the signal power reflected towards the receiver per unit solid angle to the incident power density [17], i.e., $\sigma = \lim_{R\to\infty} 4\pi R^2 \cdot \frac{P_r}{S_i}$, where P_r is reflected signal power per unit solid angle, S_i is incident power density, and R is the distance of the target. Thus, RCS is independent of the distance of the target from the radar [18]; however, it is defined in far field of the target. RCS is defined to reflect the characteristics of the target and not the effects of the transmitter power, receiver sensitivity or the distance of the target from transmitter and receiver. RCS of a target depends on various factors including shape, size, polarization, angle of contact, frequency, etc. When a radio wave falls on a target there will be reflection, diffraction and absorption whose contribution varies with the movement of the target. For instance, the polarization of the returning reflected wave is not the same as the polarization of the wave transmitted. Thus, the component of the polarization tangential to the receiving antenna will define the RCS.

The RCS of a human body is also studied in some literature. Despite the fact that the RCS changes with movement type, body orientation, body size, distance, frequency, angle of contact, etc.; the contribution of each rigid part of the body to the total RCS remains constant even during motion. The same assumption is also used throughout this thesis. In addition, the RCS can be directly related to half of the body surface area which is exposed when the person is in front of the radar [19]. This area is typically listed as $1m^2$. The 12 major parts of the human body listed in Section 2.1.1 contribute to a fraction of the RCS. The torso has the highest RCS followed by the legs and arms; while, the head and feet have the least contribution. Particularly, the percentage at which of these body parts contribute is listed as: torso 31%, left and right arms 10% each, left and right legs 16.5% each, head 9% and feet 7% [19].

2.2 Methods to characterize human motion

Once the velocity profile and RCS models of the body are defined, the question is what parameters can be extracted from these models for human movement identification or classification. Some literature states certain parameters of motion and claim that these parameters have a unique range of values for human movement and their value differs for the different types of human activities [4], [8]. However, the exact range of these parameters for such identification or classification is not yet known. This is because, coming up with a range of values for these parameters requires a detailed study of human locomotion, its kinematics and modeling the different types of human activities. Such type of modeling is challenging; moreover, the values of these parameters change significantly in

different scenarios. Despite these limitations, these parameters are used for our human movement characterization because:

- A random human movement can be divided into a uniform movement over small time durations. Thus, the value of these parameters over the small time durations can be defined.
- The classification error can be significantly decreased by training a classifier with real data of these parameters.

2.2.1 Human Movement Identification

Different parameters of movement can be selected to discriminate human movement from non-human movements. Of these parameters, the following parameters are unique enough to identify human motion from movement of other animals or objects [4].

1. ***Torso Velocity***, v_{torso}: is the velocity of the main component or trunk of the human body. This is the velocity component that has the largest RCS, σ; but the lowest velocity variation, lowest $k_{m1}, \cdots, k_{m4}$ in (2.1). Hence, the torso velocity is approximately equal to the velocity of the body, $v_{torso}(t) \approx V$. Hence, the average value of $v_{torso}(t)$ can be taken to estimate the body velocity, which is one of the parameters that has a unique range for a human target. Moreover, the way the parameter $v_{torso}(t)$ is changing with time shows the pattern of motion.
2. ***Cadence frequency***, f_c: is the rate of oscillation of the body parts. As the legs have the highest, $k_{m1}, \cdots, k_{m4}$ and hence the highest oscillation amplitude as discussed in Section 2.1.1; the cadence frequency of the legs is the most dominant oscillation. Like the torso velocity, the cadence frequency has a unique range for human motion. For instance, a cadence frequency of $10Hz$ is too fast to be expected from human motion.
3. ***Step length***, S_l**:** is the distance between the point of initial contact of one foot and the point of contact of the opposite foot. In addition to the torso velocity and the cadence frequency, the relationship between these two parameters also identifies humans uniquely. Step length is the ratio of the torso velocity to the cadence frequency, i.e., $S_l = \frac{v_{torso}}{f_c}$. The step length is one of the parameters which distinguish human movement from movement of other animals [7]. If estimated accurately, the step length can even help to discriminate male and female human subjects.

A research done on human subjects in a typical walking experiment measured using a speed graphic camera shows that these parameters for normal men and typical walking are found to be [20]:

- Torso velocity $1.54m/sec$
- Step length $0.79m$

- Cadence frequency 1.95 steps/sec.

It is also reported in [15] that an empirical relationship between the body velocity and the cadence frequency of the gait is found to be: $f_c = \frac{\sqrt{V}}{1.346}$ for typical human walking.

2.2.2 Human Activity Classification

Activity classification can be done by matching parameters extracted in a real scenario to the set of similar parameters extracted from pre-generated models for the different human activities [5]. This matching can be more automated, efficient and more accurate by training the classifier with continued experiments of each human activity that need to be discriminated. Different movement parameters are claimed to be unique from activity to activity by different researchers. The most common parameters include the following [8]:

1. ***Torso velocity & cadence frequency***: In addition to being used as identification parameters, an accurate estimation of these parameters will lead to activity classification. The magnitude of the torso velocity and the cadence frequency of the gait are expected to be different from activity to activity. For instance, the torso velocity obtained from a sitting person should be around zero; however, the torso velocity should be at least higher than $1m/sec$ for a running person. The gait pattern has a higher rate of oscillation for walking than running. This implies these two parameters can be utilized for classification.

2. ***Velocity bandwidth***: This involves the difference between the maximum and minimum velocity components that occur during a certain activity. In (2.1), the oscillation amplitude A depends on the type of motion. Some activities give a larger value of A, hence high velocity bandwidth and other activities result in a lower A, hence low velocity bandwidth. For instance, the velocity bandwidth during running is high as compared to the velocity bandwidth during crawling.

3. ***Velocity bandwidth without micro-Doppler***: This involves the velocity bandwidth due to velocity components from the torso and other body parts with low $k_{m1}, \cdots, k_{m4}$ only, i.e., without including the oscillation of legs and arms. This parameter particularly describes the velocity extremes attained by the torso during the activity. The velocity bandwidth of the torso differs from activity to activity; thus, it is one of the micro-Doppler parameters for classification.

4. ***Velocity offset***: This parameter shows the offset of the velocity profile from zero velocity. It is the measure of asymmetry of the forward and backward swings of the appendages. These swings are not symmetrical for most human movements and the asymmetry is unique. If the swings are symmetrical, then the velocity offset will be equal to the torso velocity.

Chapter 3

Doppler Shift in Indoor Environment

The basic principle behind radars measuring the speed of a target is the Doppler effect introduced by Christian Doppler in 1842 for sound waves [21]. In the first section of this Chapter, the Doppler effect and its analysis for a human target in a multipath environment is derived and analyzed in detail. The radar equation and the expected signal to noise ratio is formulated considering a general bistatic radar scenario. Special cases of this SNR in different scenarios are also evaluated.

The discussion on Doppler shift from a human body is taken into consideration to set minimum requirements on a radar system that can be used for characterizing human movement. Continuous wave and pulse Doppler radars which are commonly used by the radar community and which can be chosen for such application are discussed and compared against each other. Some additional flexibility that can be achieved in these radar types is discussed. Finally, the idea of using a pseudo random sequence instead of pulse transmission is suggested.

3.1 Doppler Effect in Radars

3.1.1 Principle of Doppler Shift

Doppler radars use the principle of the Doppler effect to measure the velocity of a target. The Doppler theory says: an electromagnetic wave hitting a moving target undergoes a frequency shift proportional to the velocity of the target. The major question is how does this frequency shift occur and how much frequency shift is expected when a target is moving with a velocity, V.

Assume the scenario shown in Figure 3.1; a human target moving at a distance, R_{tx} and at a time varying velocity, $V(t)$ in a direction that has angle θ_1 with the radial direction of the transmitting radar. Assume that these parameters with respect to the receiver radar are the distance R_{rx}, and the angle θ_2. Thus, the electromagnetic signal moves a total distance of $R_{tx} + R_{rx}$. Let's assume that this velocity vector is in a plane

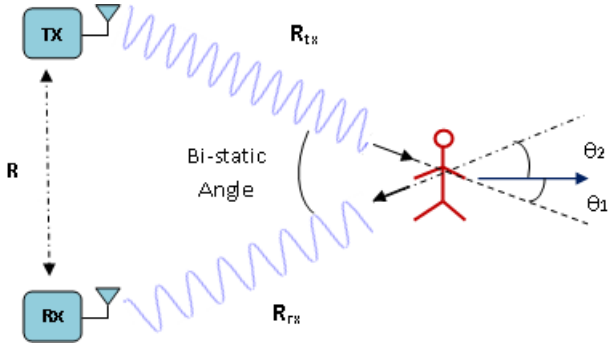

Figure 3.1: Movement of a person and Doppler radar

parallel to the floor of the room; in other words, let's assume vertical displacements are insignificant.

Assume unmodulated continuous wave (CW) signal given by; $x(t) = Ae^{j(\omega t+\phi_o)}$ is transmitted, where A is the amplitude, ω is the frequency and ϕ_o is the initial phase. The reflected echo from the human target received at the receiver antenna has a time varying amplitude, $a(t)$ and a time varying phase change, $\phi(t)$ and can be given by: $a(t)e^{j(\omega t+\phi_o+\phi(t))}$. Hence, the received baseband signal after demodulation reduces to:

$$y(t) = a(t) \cdot e^{j\phi(t)} \tag{3.1}$$

From this equation, it is clear that the frequency content of the received signal, $y(t)$ is dependent on the time varying phase. For narrowband signals, the time varying phase, $\phi(t)$ can be directly related to the delay or the number of wavelengths the wave travels. This relation is given by:

$$\phi(t) = 2\pi \cdot \frac{(R_{tx}(t) + R_{rx}(t))}{\lambda}$$

where, λ is the wavelength of the electromagnetic wave being transmitted. Thus, the Doppler frequency is given by,

$$f_d(t) = -\frac{1}{2\pi} * \frac{d\phi(t)}{dt} = -\frac{1}{\lambda} \cdot \left\{ \frac{d}{dt} R_{tx}(t) + \frac{d}{dt} R_{rx}(t) \right\}$$

This implies that the Doppler shift depends on the combined rate of change of the distances, $R_{tx}(t)$ and $R_{rx}(t)$. From this equation, it is also evident that: when the human target moves away from the radar, that is when the distances $R_{tx}(t)$ and $R_{rx}(t)$ increase, the Doppler frequency is negative; and when the person moves towards the radar, the Doppler frequency is positive.

Hence, a target moving at an angle θ_1 with respect to the direction of the signal from the Tx antenna and θ_2 from the Rx antenna as shown in Figure 3.1 has a Doppler shift given by:

$$f_d(t) = \frac{V(t)}{\lambda} \left[\cos(\theta_1) + \cos(\theta_2)\right] \tag{3.2}$$

(3.2) implies that a radar measures the radial component of the velocity of the target. Thus, the Doppler shift is dependent not only on the velocity of the target, but also on the relative position of the radar transmitter and receiver with respect to the target.

The received baseband signal, $y(t)$ can also be expressed in terms of the velocity of the target. Doppler frequency of a human target is time varying; thus, the received signal should be analyzed in a time fraction of the motion, Δt that is short enough to assume uniform motion (constant Doppler frequency). That is, a random human motion can be divided into short intervals of uniform motion. This allows to express the phase, $\phi(t)$ locally as: $\phi(t) = 2\pi f_d \cdot t + \phi_o$, where ϕ_o is the initial phase at the start of the time interval, Δt. The amplitude, $a(t)$ can also be assumed constant during short time intervals. Therefore, the received signal, $y(t)$ can be expressed locally as :

$$y(t) = a.e^{j(2\pi f_d t + \phi_o)} \tag{3.3}$$

3.1.2 Doppler Shift and Radar Configurations

A general radar system with separate transmitter and receiver sections is shown in Figure 3.1. A radar system may consist of a single transceiver instead of a separate Tx and Rx. There can also be a case in which the radars are placed on opposite directions with respect to the target. In general, radar systems are classified into different configurations based on the relative position of the transmitter and receiver. These classifications are based on the bi-static angle, the angle subtended between the transmitter, target and receiver as shown in Figure 3.1 .

***Monostatic*:** is a radar system in which the transmitter and receiver are collocated or the bistatic angle is exactly 0°. In this radar system a single antenna is commonly used together with a duplexer to isolate the sensitive receiver from the high power transmitter.

***Pseudo-monostatic*:** is a radar system in which the bistatic radar is close to 0°. Pseudo-monostatic[1] consists of an independent transmitter and receiver placed at a distance much smaller than the distance to the target, that is $R \ll R_{tx} \& R_{rx}$. This is the radar configuration used in this thesis due to limitations of the platform discussed in Section 6.3.

***Bistatic*:** If the bistatic angle is much higher than 0°, then the configuration is called bistatic radar. One special case of bistatic radar is when the bistatic angle is 180^o. This radar configuration is called forward scatter radar.

The effect of human motion on the Doppler frequency is different in these radar configurations as (3.2) shows.

[1] It is the radar configuration used in most of our experiments.

- For pseudo-monostatic radar, $\theta_1 = \theta_2 = \theta$. Thus, (3.2) reduces to: $f_d = 2\frac{V}{\lambda}\cos(\theta)$. In monostatic radars, this equation further reduces to: $f_d = 2\frac{V}{\lambda}$. For pseudo-monostatic radars also $R \ll R_{tx}\&R_{rx}$; thus, $\theta \approx 0$. Therefore, it is assumed throughout this thesis that $f_d = 2\frac{V}{\lambda}$ holds for pseudo-monostatic radar configurations. The Doppler shift is doubled; thus, it is significant in monostatic and pseudo-monostatic radar configurations. However, the major challenge is the strong direct path signal from Tx to Rx antenna.

- In bistatic radars, the bistatic angle is much larger than 0°. A special case occurs for the forward scatter radar where $\theta_1 = 180 - \theta_2$. In this case, (3.2) reduces to $f_d = \frac{V}{\lambda}\left[\cos(180 - \theta_2) + \cos(\theta_2)\right] = 0$. Thus, the Doppler shift in bistatic radar configurations is not significant as compared to that of the monostatic radars in general.

One of the factors that make the indoor environment different from the outdoor ones is the presence of multipath. Due to the presence of multipath, the Doppler shift in bistatic radars will be actually much higher than zero.

3.1.3 Clutter in an indoor Environment

Clutter is a term given to the reflected signal from unwanted objects in the environment. Clutter can be divided into moving clutter and stationary clutter. Moving clutter can be caused by wind, moving house equipments such as fan, doors, etc. However, stationary clutter can be caused by wall, ceiling, ground, room furniture, etc. In indoor environments both types of clutter could exist.

- If the Doppler frequency from the moving clutter is much higher than humans, then it will be filtered out by the receiver. Otherwise, the assumption is moving clutter can be discriminated from human movement by using the movement identification parameters.

- Stationary clutter does not cause a Doppler shift; thus, the frequency of this clutter is the same as the frequency of the direct signal from Tx to Rx. Therefore, stationary clutter contributes to the power of the direct signal.

3.1.4 Doppler Shift in Multipath Environment

For a person moving at a velocity, V in a pseudo-monostatic radar configuration, the Doppler shift is given by: $f_d = \frac{2V}{\lambda}$. Thus, received signal in (3.3) can thus be expressed in terms of the target velocity as:

$$y(t) = a.e^{j(\frac{4\pi V}{\lambda}t + \phi_o)} \tag{3.4}$$

The human body is not a rigid body; thus, the body can be divided into M rigid body parts. Each body part makes a frequency modulation of the transmitted signal due to the time varying velocity profile. Thus each body part, m is described by:

- a RCS, σ_m
- a velocity, $v_m(t)$ expressed in (2.1).

Assume that there is a single ray that reflects back from each body component. Thus, the Doppler signal model during short time intervals of the motion, shown in (3.4) can be expressed as a superposition of the M body parts as follows:

$$y(t) = \sum_{m=1}^{M} \sqrt{\sigma_m} \cdot a \cdot e^{j(\frac{4\pi v_m}{\lambda} t + \phi_m)} \tag{3.5}$$

In a multipath environment, such as an indoor environment, there will be more than one ray between the person and the radar as Figure 3.2 shows. Some paths may involve a reflection of the person only; whereas, other paths involve more reflections of surrounding walls and objects. Thus, there will be more than one ray going to each of the body parts. Moreover, the number of these multipath is time varying as the person is in transition. Let's assume their are R paths involving the transmitter, the person and the receiver during the time fraction,Δt for each body part[2]. Each of these rays, r is described by:

- a velocity profile for each body part, $v_{mr}(t)$.
- an initial phase ϕ_{mr}, corresponding to the initial position of each body part with respect to each ray when the motion starts.
- a magnitude, $a_r(t)$, that is an inverse function of the path length of each ray.

Each body part has different angle of contact with respect to each ray, thus the RCS will be dependent on the ray, r. Therefore, the received signal involving multipath will be given by,

$$y(t) = \sum_{m=1}^{M} \sum_{r=1}^{R} \left[\sqrt{\sigma_{mr}} \cdot a_r \cdot e^{j(\frac{4\pi v_{mr}}{\lambda} t + \phi_{mr})} \right] \tag{3.6}$$

However, the product $\sqrt{\sigma_{mr}} \cdot a_r \cdot e^{j\phi_{mr}}$ can be written as a single complex number, β_{mr} and the exponent $\frac{4\pi v_{mr}}{\lambda}$ as ω_{mr}. Hence, the received Doppler signal model during a short time interval, Δt can thus be expressed as:

$$y(t) = \sum_{m=1}^{M} \sum_{r=1}^{R} \left[\beta_{mr} \cdot e^{j\omega_{mr} \cdot t} \right] \tag{3.7}$$

The idea shown by (3.6) can also be justified using Figure 3.2. The figure shows the direction and magnitude of the radial velocity of the person with respect to each ray is different. For instance, the person is moving towards the radar based on ray-1; while he is moving away from the radar based on ray-2. This effect creates image frequencies,

[2]The number of paths also depends on the position of the body parts. It is obvious that there will be more number of paths to the torso than to the feet; however let's assume all have n paths.

Doppler frequencies of smaller magnitude which are positive when the person is moving away and negative when the person is moving towards the radar. Therefore a wide velocity spectrum[3] will be created even though the person moves at constant velocity.

The other factor that leads to wide velocity spectrum is the fact that the rigid components of the human body constitute a continuous range of velocities. As discussed in Section 2.1, the parts of the body move at different velocities superimposed on the velocity of the main body and each part will have a velocity range between its nearest and farthest ends. Hence, this effect also creates an increase of velocity spectrum width.

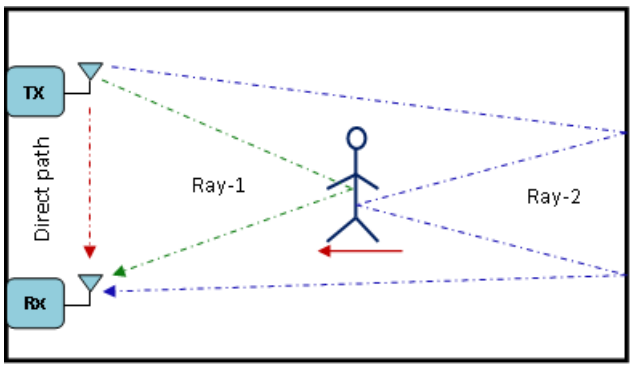

Figure 3.2: Doppler Effect in a multipath environment

3.2 Radar Equation and SNR

(3.1) shows that it is not only the phase of the signal that is time varying but also the amplitude. The major reason for this change in amplitude is the path loss. As the position of the person changes, the total distance the reflected wave travels changes and that means the path loss changes.

Let's consider the amplitude variation, $a_r(t)$ of the multipath components due to free space path loss. That is, if a power, P_t is transmitted; how much power or signal to noise ratio is received. The equation that describes this relationship is commonly called the "Radar Equation". The radar equation shows the power of the signal received as a function of the characteristics of the radar system and the characteristics of the target.

Assume a general scenario shown in Figure 3.1. The power density, S_t radiated from the transmitter radar at a distance, R_{tx} is thus given by:

$$S_t = \frac{P_t \cdot G_t}{4\pi \cdot R_{tx}^2}$$

where: G is the gain of the transmit and receive antennas (let's assume identical antennas are used).

[3] A velocity profile consisting of a wide and dispersed range of velocities.

This radiated power density is intercepted by the human target of RCS, σ resulting in a received signal that is radiated back to the receiver with a power density:

$$S_r = \frac{S_t \cdot \sigma}{4\pi \cdot R_{rx}^2} = \frac{P_t \cdot G_t \cdot \sigma}{(4\pi.R_{tx}.R_{rx})^2}$$

This will be again intercepted by the effective area of the receiver antenna, A_e which can be expressed in terms of the gain of the receiver antenna, G as $Ae = \frac{G \cdot \lambda^2}{4\pi}$ where, λ is the wavelength of the wave being transmitted.

Assume the receiver has a controllable gain G_R in the RF section; the received signal power is then given by:

$$P_r = \frac{P_t \cdot G^2 \cdot \lambda^2 \cdot \sigma \cdot G_R}{(4\pi)^3 \cdot (R_{tx} R_{rx})^2} \tag{3.8}$$

The noise power consists of two parts: the thermal noise and the phase noise due to leakage of the Tx signal into the Rx. The thermal noise is given by ,

$$N_{thermal} = K \cdot B \cdot T \cdot F \cdot G_R$$

where K is the Boltzmann's constant , B is the bandwidth of the receiver, T is room temperature and F is the noise figure of the receiver.

The phase noise, N_{phase} of the receiver is frequency dependent and it can obscure the velocity information from slowly moving targets. Phase noise in Doppler radars is analyzed in detail in [22] and is expressed as:

$$N_{phase} = \int_B [P_t \cdot L_p \cdot G_R \cdot L_{phase}(f)]\, df$$

where, L_p is the circuit or antenna isolation between Tx and Rx parts of the radar. It describes what fraction of the transmitted power leaks directly into the receiver circuit. $L_{phase}(f)$ is the single side band (SSB) phase noise[4] spectrum that results when the transmitted signal is mixed with the receiver local oscillator. This parameter is relevant as the effect of the direct signal is not only at the transmission frequency but also on the surrounding frequencies with reduced effect. Thus, the total noise $N = N_{thermal} + N_{phase}$ is given by;

$$N = K \cdot B \cdot T \cdot F \cdot G_R + \int_B P_t \cdot L_p \cdot G_R \cdot L_{phase}(f) df$$

Hence, the received Signal to Noise Ratio (SNR) is given by,

$$SNR = \frac{P_r}{N} = \frac{P_t G^2 \lambda^2 \sigma}{(4\pi)^3 (R_{tx} R_{rx})^2 \cdot \left(KBTF + \int_B P_t L_p L_{phase}(f) df\right)} \tag{3.9}$$

Thus, when the distances R_{tx} and R_{rx} vary due to movement of the person; the SNR varies accordingly. The SNR expression shown can further be reduced in two scenarios:

[4]SSB phase noise is the phase noise spectrum at a given frequency offset expressed in decibels relative to carrier per hertz, dBc/Hz .

1. When the phase noise is significant, for instance for the case of an asynchronous transmitter and receiver consisting of an ordinary, high ppm[5] oscillator. In this case, $N_{thermal} \ll N_{phase}$. Thus, the SNR reduces to:

$$SNR = \frac{G^2\lambda^2\sigma}{(4\pi)^3 (R_{tx}R_{rx})^2 L_P \int_B L_{phase}(f)df}$$

This implies that the SNR cannot be increased by increasing the transmit power when the phase noise is significant.

2. When Phase noise on the received signal is negligible, for instance, for the case when both the transmitter and receiver use a stable low ppm reference oscillator. In this case, $N_{thermal} \gg N_{phase}$, and we obtain:

$$SNR = \frac{P_t G^2\lambda^2\sigma}{(4\pi)^3 (R_{tx}R_{rx})^2 (KBTF)} \tag{3.10}$$

(3.9) shows that the variation in amplitude of the received signal is due to the change in distance of the target. This equation describes the SNR of each multipath ray as a function of the distance of the target with respect to each ray. However, what matters most is ratio of the power of each multipath ray which carries information to the power of the direct signal between the Tx and Rx. This ratio is described as follows.

Let's take again the radar scenario shown in Figure 3.1 with the line of sight distance between Tx and Rx denoted by R. The power of the direct signal received from transmitter to receiver antenna, P_{direct} can be expressed as: $P_{direct} = \frac{P_t G^2\lambda^2}{(4\pi R)^2}$. The signal reflected from the human target and received at the Rx is described by (3.8). Then, the ratio of the reflected power to the direct path power is given by:

$$Ratio = \frac{P_{reflec.}}{P_{direct}} = \frac{\sigma}{4\pi} \cdot \left(\frac{R}{R_{tx} \cdot R_{rx}}\right)^2$$

Hence, the magnitude of the reflected signal as compared to the magnitude of the direct signal is expressed in dB as;

$$Ratio|_{dB} = 10 \cdot \log(\sigma) + 20 \cdot \log\left(\frac{R}{R_{tx}.R_{rx}}\right) - 10 \cdot \log(4\pi) \tag{3.11}$$

Figure 3.3 shows this ratio for $R_{tx} = R_{rx} = 5m$ and $\sigma = 1$; the reflected signal will be much less than the direct signal as the Tx and Rx are placed more closely. The ratio decreases further as the distance of the target, $R_{tx} + R_{rx}$ increases. This ratio can be improved by using directional antennas to minimize the direct signal.

For the multipath rays which carry information, the direct path power can also be considered as a phase noise with isolation, L_p equal to the path loss. Thus, the major

[5]Parts per million(ppm) is a measure that shows how much an oscillator may drift from the designated oscillating frequency

cause of phase noise in the receiver depends on which of the isolation: the circuit isolation or the antenna isolation is weaker.

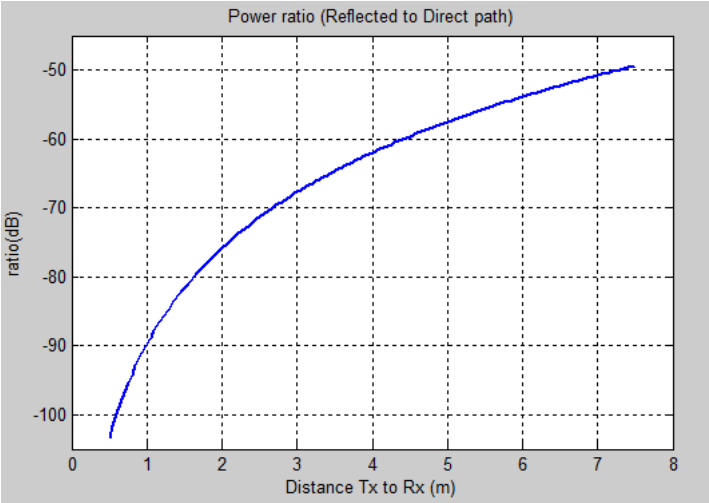

Figure 3.3: Ratio of reflected to direct signal

3.3 Requirements for Human Movement Characterization

Architectural complexity and cost of a radar system grows as the application requires more bandwidth, resolution, accuracy, etc. On the other hand, the requirements should be satisfactory enough for the application concerned. For human movement characterization, the minimum requirements of a radar system are set taking into consideration the properties of human movement parameters introduced in Chapter 2.

Maximum Doppler: The velocity of a person in an indoor environment varies from time to time. For most activities that human beings perform, the velocity of motion varies throughout the activity and depends on many factors; moreover, different parts of the body move with different velocities of varying magnitudes. However, at normal conditions a maximum velocity of $5m/sec$ can be set reasonably. This maximum velocity corresponds to a maximum Doppler frequency of, $fd_{max} = 2 \cdot \frac{Vr_{max}}{\lambda} = 167Hz$[6]. Adding some confidence interval, the maximum Doppler frequency is set to $200Hz$.

Frequency Resolution: As described in Section 3.1.4, a range of velocities of different magnitude exist even when the body moves at constant velocity. Thus, the velocity resolution should be good enough to resolve these micro-Doppler[7] signatures of the movement. However, velocities less than $5cm/sec$ can reasonably be taken as

[6] assuming a carrier frequency of 5GHz($\lambda = 0.06$) is used

[7] Micro-Doppler refers to the reflected Doppler frequency pattern obtained from non-rigid body movement.

no movement. Therefore, it is assumed that a velocity resolution of $5cm/sec$ is required. These velocity resolution corresponds to a Doppler frequency resolution of,$\Delta fd = 2 \cdot \frac{\Delta Vr}{\lambda} = 1.6Hz$. This shows that a typical frequency resolution of $1Hz$ will suffice.

Time Resolution: In order to identify and classify activity, the variability of the micro-Doppler signatures should be monitored. The motion within a time window equal to the time resolution should be stationary[8]. This time window should be small enough to avoid abrupt velocity changes due to acceleration of parts of the body and should be large enough to avoid computational complexity. Human movement model, Section 2.1.1, should thus be considered in order to determine this parameter. Therefore, the required time resolution is set to $0.2sec$ considering these factors.

Bandwidth: Assume that there is only a single mover and the change in the received signal is due to the human activity concerned only. Provided these assumptions are true; the bandwidth requirement is thus determined by the maximum Doppler frequency expected, $200Hz$. Hence, a bandwidth of $200Hz$ is assumed.

Sampling frequency: We need to distinguish approaching and receding targets; thus, the sampling frequency should be set at least twice the bandwidth required. Therefore, a sampling frequency of $2.5 * Bandwdith = 500S/sec$ is selected.

Thus, the following minimum requirements are required for characterizing human activity based on Doppler shift:

- Maximum Doppler of 200Hz.
- Frequency resolution of 1Hz.
- Time Resolution of 0.2sec.
- A bandwidth of 0.5KHz.

3.4 Radar Types

As highlighted in the purpose of the thesis, the starting point in this thesis is to select a radar technology which can be used for characterizing human movement; then, to investigate which of these radar types can be implemented using a general purpose low cost hardware.

There are different radar architectures which can possibly be used for monitoring human movement. These architectures differ from each other in their transmission waveforms, bandwidth requirement, the way to separate transmission and reception, implementation complexity, the parameters that can be estimated, etc.

[8]A motion (the Doppler signal that result from it) is stationary if its expectation is independent of time and its auto-correlation function $E[x(t_1).x(t_2)^*]$ depends only on the time difference $t_2 - t_1$.

3.4.1 Unmodulated Continuous Wave (CW) Radar

Radar engineers commonly use the name "continuous wave" for a transmission that is continuous through time or a non-pulse transmission. CW radars may be modulated as in FMCW [17] radars or they may be unmodulated CW radars. In the sections that follow, unmodulated CW radars are discussed; so these radars are simply denoted as CW radars.

In CW radars a carrier is transmitted. A portion of the radiated energy of this carrier is reflected back from the moving target with a Doppler frequency shift. Then, the received echo signal will be mixed with the reference signal from the transmitter. The resulting output will then be filtered with a matched filter to obtain the velocity of the target. CW Radar has the following properties in general:

- It is a radar system with small Tx and Rx complexity.
- CW radar has no means to measure the time of arrival of the signal or the range of the target, since there is no modulation of a distinct waveform.
- The high power Tx is operating at the same time with the low power Rx. The strong direct signal from the Tx affects the Rx; therefore, proper isolation is required between Tx and Rx sections.
- Two targets cannot be spatially resolved using CW radar. In other words, the signal received by this radar is the sum of all the reflections from targets at various distances.
- There is no velocity ambiguity in CW radars.

The need to resolve multiple targets and isolate indoor reflections from the outdoor ones leads to the idea of using pulse Doppler radar.

3.4.2 Pulse Doppler Radar

Transmission of a modulated pulse instead of an unmodulated carrier enables the measurement of a target's location. In these radars, pulses of a low duty cycle are modulated and sent by the Tx. Then, the time of arrival of the reflected echo is estimated in order to measure the target's range. In addition, the Doppler shift between the frequency of the modulating carrier and the frequency of the reference signal enables measurement of the velocity of the target.

The range resolution, the minimum distance at which two closely spaced targets can be resolved, is proportional to the bandwidth of the pulse, B. For monostatic radars, it is given by [17],

$$\Delta R = \frac{C}{2B} \tag{3.12}$$

where C is the speed of light. (3.12) implies that to resolve very closely spaced targets, such as the reflections from the parts of a human body, ultra-wideband radars are required.

The other important parameter of a pulse Doppler radar is pulse repetition frequency (PRF). Pulse repetition frequency limits the maximum range that can be measured; because of ambiguity with reflection of the next pulse. In order to measure a maximum distance of R_{max}; the PRF must satisfy $PRF < \frac{C}{2R_{max}}$ [17]. However, a low PRF creates a velocity ambiguity on the other hand since the Doppler shift will be aliased with shift of the next frequency in the spectrum. Hence, to avoid velocity ambiguity (aliasing), the PRF must satisfy $PRF > 4\frac{V_{max}}{\lambda}$ [17]. Hence, the PRF must be designed such that both ambiguities are compromised if the Doppler radar is to be used for measurement of both range and velocity. For the purpose of human movement characterization range is not important; thus, the PRF can be set as high as the hardware allows.

Pulse radar can be implemented in two ways,

- The first way which is widely used by the radar community is using a single antenna with a duplexer. In between each pulse, the radar system switches to reception mode to receive the reflected echo from the target. This gives the radar the freedom to send high transmit power to increase the received SNR. However, this radar implementation suffers from a "blind zone", the range till which the radar will not receive target reflections. That means the range profile of the radar starts from the radar blind zone, $R_{blind} = \frac{C}{2 \cdot B} = \frac{C.PW}{2}$ (where PW is the pulse width) , and ends at the maximum distance, R_{max}. Thus, this method requires a fast switching hardware that can also generate a short pulse.

- The second way is using separate sections as Tx and Rx and enabling transmission and reception at the same time, so that reception is possible from the instant transmission is started. This implementation avoids the radar blind zone. Thus, it is suitable for indoor applications; however, it suffers from low average SNR. In addition, high transmit power cannot be used due to the sensitive Rx operating simultaneously in the vicinity of the Tx.

As discussed above, pulse radar has generally a low average SNR. The need to increase the received SNR initiates the idea of transmitting a modulated sequence and processing the received sequence to obtain a short pulse so that the same spatial resolution is obtained, the process called pulse compression. Pulse compression can be achieved by modulating a carrier with pseudo random sequence (PRS) or a linear frequency modulation (chirp).

3.4.3 Pseudo-random sequence (PRS) Radar

In PRS radar, a carrier is phase modulated with a periodic pseudo random sequence of degree p (a p-sequence) and of length, $J = 2^p - 1$. A Pseudo-random sequence is a binary phase shift keying (BPSK) sequence, $s\,[j]$ having auto-correlation, $A[n]$:

$$A[n] = \frac{1}{J}\sum_{j=1}^{J} s\,[j]\,.s\,[j-n] = \begin{cases} 1 & ,\ n = 0 \\ \leq \frac{1}{J} & ,\ otherwise \end{cases}$$

This sequence is random but repeats itself after a length, J; hence the name "pseudo random". PRS radar sends the sequence and correlates shifted versions of the received

sequence with the reference to get the channel impulse response. As compared to a single pulse, this sequence has higher average SNR.

A pseudo random BPSK signal of length J is transmitted. A signal of length, $K + L_I - 1$: $y[0], y[1], \cdots ., y[J + L_I - 2]$, is received, where L_I is the length of the impulse response of the channel. L_I must be taken as large as J, in order to compute the resulting impulse response though all shifts of the sequence. In matrix form, this can be given by, $y = \mathbf{S}h$, where: $\mathbf{S}$ is a toeplitz matrix consisting of the transmitted BPSK sequence and h is the impulse response of the channel.

$$\begin{bmatrix} y_0 \\ \vdots \\ y_{J+L-2} \end{bmatrix} = \begin{bmatrix} s_0 & s_{J-1} & \cdots & s_1 \\ s_1 & s_0 & \cdots & s_2 \\ \vdots & & \ddots & \vdots \\ s_{J-1} & & & s_0 \\ s_0 & s_{J-1} & & \vdots \\ \vdots & & \ddots & s_{J-1} \end{bmatrix} * \begin{bmatrix} h_0 \\ \vdots \\ h_{L_I-1} \end{bmatrix}$$

Assuming the channel matrix is deterministic for short time intervals, the BLUE (best linear unbiased estimator) can be used to estimate h. That is,

$$h = \mathbf{S}^{+}y = \left(\mathbf{S}^{H}\mathbf{S}\right)^{-1}\mathbf{S}^{H}y$$

Then, the maximum value from the h vector is selected among the L_I paths as the path that contain movement. The variation of the impulse response with time is then analyzed to obtain movement information. If the radar is wideband (if there is good spatial resolution), then the person will cover many bins in his motion. In that case, a combined analysis of more than one bin and tracking of the bins that contain movement may be required.

Chapter 4

Time-Frequency Estimation

In order to estimate the time varying Doppler frequencies described by (3.7), spectral estimation techniques will be used. Non-parametric spectral estimators such as the discrete Fourier transform (DFT) are good estimators as long as the frequencies to be estimated are well-separated; however, high resolution parametric spectral estimators are required to resolve closely spaced frequencies. In this Chapter, non-parametric and parametric spectral estimators are introduced. Joint time-frequency estimation is discussed as a means to see the variability of the signal in both time and frequency dimensions by using these estimators. The optimal parameters selected in the joint time-frequency estimations for parametric and non-parametric estimators are described. Background spectral subtraction is discussed as a means to facilitate the extraction of human movement parameters after spectral estimation.

However, before applying the aforementioned spectral estimation techniques it is necessary to pre-process the signal which involves I-Q imbalance correction and decimation.

Finally, we discuss a simple but important technique to estimate the change in phase of the signal sample by sample, the so-called quadrature demodulation method, is discussed.

4.1 Signal pre-Processing

Before the spectrum of the signal is estimated some artifacts in the signal should be removed. Firstly, most signal processing methods assume that the In-phase (I) and Quadrature (Q) signals are equal in amplitude and have a phase shift of 90°. However, this phase and amplitude relationship of the I and Q signals may not be as expected due to receiver circuit artifacts. Therefore, I-Q imbalance correction should be carried out. Secondly, the signal received from analog to digital converters could be of higher sampling rate than the rate required for Doppler analysis. Moreover, the signal contains high frequency components. Therefore, the signal should be low-pass filtered and decimated to the required sampling rate before further processing.

4.1.1 I/Q Imbalance Correction

Let's assume that the imbalanced I and Q signals are given by, $I = A.\cos(\omega t + \theta_o)$ and $Q = B.\sin(\omega t + \theta_o + \phi_e)$ where, $r = \frac{A}{B}$ is the amplitude error and ϕ_e is the phase error.

To correct these errors, let's expand $r \cdot Q$ and form a corrected Q: $Q_{new} = A.\sin(\omega t + \theta_o)$ from this expansion.

$$\begin{aligned} r \cdot Q &= A \cdot \sin(\omega t + \theta_o + \phi_e) \\ &= A \cdot \sin(\omega t + \theta_o) \cdot \cos(\phi_e) + A \cdot \cos(\omega t + \theta_o) \cdot \sin(\phi_e) \\ &= Q_{new} \cdot \cos(\phi_e) + I \cdot \sin(\phi_e) \end{aligned}$$

Hence, the new I and Q signals can be formed as,

$$I_{new} = I \text{ and } Q_{new} = \frac{r.Q - I.\sin(\phi_e)}{\cos(\phi_e)}$$

Note that, estimates of r and ϕ_e can be obtained by transmitting a modulated sinusoid from the radar and receiving the reflection of the same sinusoid for a static (no movement) condition. This flexibility to transmit any waveform is the major advantage of a GNU Radio based radar. The ratio of amplitudes, r can be obtained from the maximum amplitudes of the received I and Q signals and ϕ_e can be obtained from their cross correlation.

4.1.2 FIR Filtering and Decimation

In order to decimate the signal by factor D, it is more efficient[1] to use cascaded decimators than decimating with one stage, particularly if D is large. As derived in [23], an optimum number of stages can be obtained which minimized the number of computations. For a two stage decimator, a more efficient implementation can be made by dividing a decimation factor of D into decimation factors $D_1$and D_2 where,

$D_1 = \frac{2 \cdot D\left(1 - \sqrt{D \cdot \frac{\Delta f}{(2-\Delta f)}}\right)}{2 - \Delta f(D+1)}$ and $D_2 = D/D_1$; $\Delta f = 1 - \frac{f_p}{f_c}$,

where, f_p is a pass-band frequency and f_c is a cut-off frequency required at the final stage of decimation.

In our radar, a decimation factor of $D = 1000$ is required as discussed in 6.4.2. f_p is set to the maximum Doppler required ($200Hz$) and f_c is set to $250Hz$ (half of the sampling frequency). This, leads to a decimation factor of 100 and 10. Type-I FIR Filters of order 30 are used as cascaded decimators as shown in Figure 4.1 (the red box shows the frequency band till the cut-off frequency).

[1] More efficient in terms of the number of additions and multiplications needed.

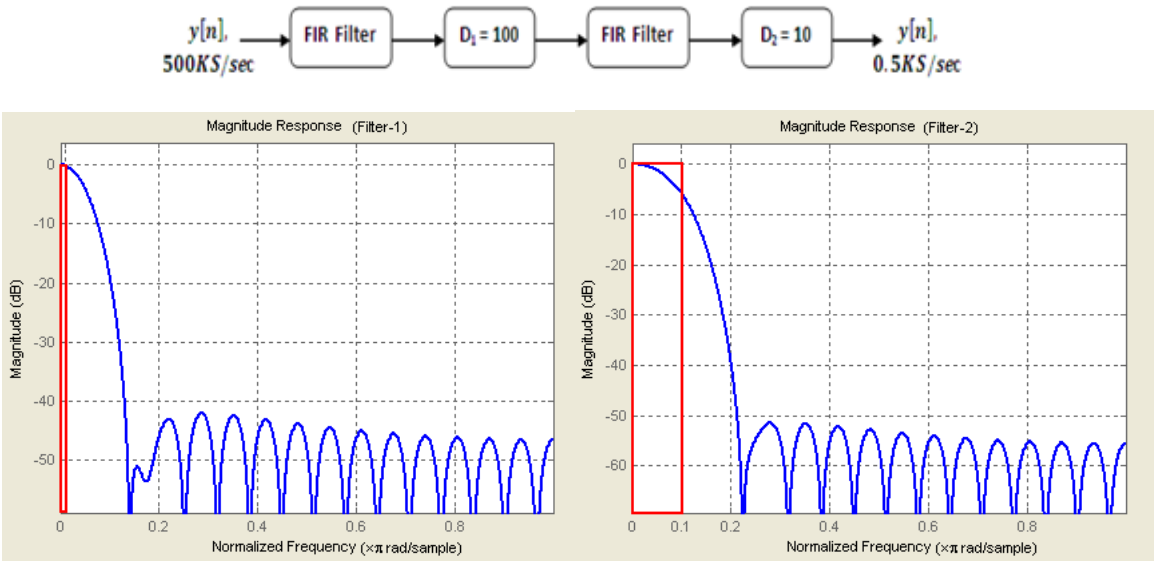

Figure 4.1: Cascaded decimation stage and FIR filter frequency response

4.2 Non-Parametric Frequency Estimation

Non-parametric spectral estimators estimate frequency content without assuming any structure on the signal. The most common spectral estimator is the periodogram, which is equivalent to the correlogram when a biased covariance matrix estimate is used.

Let's assume that, there are N samples of the received signal, $y_n : \{y[0], y[1], \cdots, y[N-1]\}$ that are available for estimation. The periodogram spectral estimator is given by [24];

$$\hat{\phi}_p(\omega) = \frac{1}{N}\left|\sum_{n=0}^{N-1} y[n]\, e^{-j\omega n}\right|^2$$

This periodogram is the same as a correlogram estimator, $\hat{\phi}_c(\omega) = \sum_{k=-(N-1)}^{N-1} w(k)\hat{r}(k)e^{-j\omega k}$ estimated using a biased auto-covariance sequence estimate, $\hat{r}[k] = \frac{1}{N}\sum_{n=k}^{N-1} y[n]\, y^*[n-k]$, where $0 \leq k \leq N-1$ and $\hat{r}[-k] = \hat{r}^*[k]$ (proof in [24]). This estimate however introduces a bias $\frac{|k|}{N}$. Thus, $\hat{r}[k]$ will be a poor estimate of $r[k]$ for values of k close to N. Thus, the solution is to weigh the auto-covariance estimate using a window so that values of k close to N will have less effect on the periodogram estimate. This windowed correlogram estimator and is given by, $\hat{\phi}_c(\omega) = \sum_{k=-(L-1)}^{L-1} w_c[k]\,\hat{r}[k]\, e^{-j\omega k}$, where $w_c[k]$ is an even windowing function which decays smoothly to zero and $L \leq N$. This lag window[2] of the correlogram can be replaced by an equivalent temporal window, $w[n]$ of length L for the periodogram and the periodogram can be given by: $\hat{\phi}_p(\omega) = \frac{1}{N}\left|\sum_{n=0}^{N-1} w[n]\, y[n]\, e^{-j\omega n}\right|^2$.

[2]It is called lag window since it weighs lags of the auto-covariance sequence

However, the periodogram is commonly computed at discrete frequency points, $\omega_k = \frac{2\pi}{N}k$, where $k = 0, 1, 2, \cdots, N-1$, which reduces the computation to windowed DFT. The DFT can be computed in an efficient way using Fast Fourier Transform (FFT).

$$Y[k] = \sum_{n=1}^{N} y[n]\, w[n]\, e^{-j\frac{2\pi}{N}kn}$$

The power spectral density (PSD) can then be estimated from the DFT using,

$$\hat{\phi}_p[\omega_k] = \frac{1}{N}\,|Y[k]|^2$$

The frequency resolution of the periodogram depends on the width of the main lobe of the windowing function. The DFT of the window, $W[\omega]$ has a width of $\frac{2\pi}{N}$ if it is a rectangular window. Hence, the resolution of the periodogram depends on the data length, N and it is basically given by: $\frac{2\pi}{N}$.

4.3 Parametric Frequency Estimation

Parametric spectral estimators assume some structure of the signal in order to estimate the frequency components. In particular, the received signal should be modeled as a sum of sinusoids. The Doppler signal model discussed in Chapter 3 can be utilized in parametric spectral estimators to estimate the frequency components of the signal. MUSIC and ESPRIT [24], are the most accurate of the available spectral estimators and are based on singular value decomposition of the auto-covariance matrix.

4.3.1 Signal Model

It is discussed in Chapter 3 that the received Doppler signal is consists of many of sinusoids whose amplitude, and frequency varies with time. The various frequency components in the Doppler signal are created due to multipath and the range of velocities from the different parts of the human body. However, the Doppler signal model is expressed as a sum of sinusoids in (3.7) by dividing the motion into parts that can be considered piecewise stationary for a time duration, Δt.

(3.7) shows that the received signal involves a summation over the number of multipath, R and the number of body parts, M. Let's represent the total number of summations, $M \cdot R$ as D. Therefore, the discrete signal model for short segments of the signal can be given by:

$$y[n] = \sum_{k=1}^{D} \left[\beta_k \cdot e^{j(\omega_k n)}\right] \tag{4.1}$$

Then, assuming a white noise, $e[n]$ is added to the Doppler signal ; the model is expressed as:

$$y[n] = x[n] + e[n] = \sum_{k=1}^{D} \left[\beta_k \cdot e^{j(\omega_k n)}\right] + e[n] \tag{4.2}$$

4.3.2 MUSIC

MUSIC (Multiple Signal Classification) is a good spectral estimation technique as compared to periodogram as it provides a frequency resolution independent of the length of the signal available for estimation.

Let's take the signal model given in (4.1), $y[n] = \sum_{k=1}^{D} \left[\beta_k \cdot e^{j(\omega_k n)}\right]$ which contains D frequency components. Let's consider a covariance matrix, $\mathbf{R}$ which can be estimated for m lags as:

$$\mathbf{R} = E\left\{y_n y_n^H\right\}$$

where $y_n = [y[n], y[n-1], \cdots, y[n-m+1]]^T$. Let $\mathbf{A}$ be a matrix consisting of frequency components to be estimated: $\mathbf{A} = [a[\omega_1], a[\omega_2], \cdots, a[\omega_D]]$ where, $a[\omega_k] = \left[1, e^{-j\omega_k}, \cdots, e^{-j(m-1)\omega_k}\right]^T$. This matrix has rank D, provided $m \geq D$ [24].

In white noise of variance σ , the covariance matrix, can be expressed as: $\mathbf{R} = \mathbf{APA}^H + \sigma^2\mathbf{I}$, based on the signal model given in (4.2), where: $\mathbf{P}$ is a diagonal matrix consisting of the power of the sinusoids: $\left\{\beta_1^2, \cdots, \beta_D^2\right\}$.

This shows there will be D eigen values larger than σ^2 of the m eigen values. Let $\mathbf{S}$ be a matrix consisting of the orthonormal eigen vectors associated with the highest D eigen values of $\mathbf{R}$ and let $\mathbf{G}$ consist of the eigen vectors of the remaining $m - D$ eigen values of $\mathbf{R}$. Thus: $\mathbf{RG} = \sigma^2\mathbf{G} = \mathbf{APA}^H\mathbf{G} + \sigma^2\mathbf{G}$. This shows that the matrix $\mathbf{A}$ satisfies the property, $\mathbf{A}^H\mathbf{G} = 0$.

Thus, the values of ω: $[\omega_1, \cdots, \omega_D]$ can be found as the highest D maxima of the cost function:

$$\frac{a^H(\omega)a(\omega)}{a^H(\omega)\mathbf{G}\mathbf{G}^H a(\omega)}$$

Thus, MUSIC has better resolution than periodogram in general. Moreover, the frequency resolution of MUSIC is independent of the data length, N. However, the estimation accuracy is dependent on N.

The eigen value decomposition of $\mathbf{R}$ is equivalent to the singular value decomposition of the data matrix, $\mathbf{X}$. The correlation matrix can be estimated as: $\hat{\mathbf{R}} = \frac{1}{N}\sum_{t=m-1}^{N-1} y_n y_n^H$ where: $y_n = [y[n], \cdots, y[n-m+1]]^T$ or $\hat{\mathbf{R}} = \frac{1}{N}\sum_{t=m-1}^{N-1} y_n^H y_n$ where: $y_n = [y[n-m+1], \cdots, y[n]]$ [24]. The data matrix for the latter is formed as:

$$\mathbf{X} = \begin{bmatrix} y[0] & \cdots & y[N-m] \\ \vdots & \ddots & \vdots \\ y[m-1] & \cdots & y[N] \end{bmatrix}$$

4.3.3 ESPRIT

ESPRIT (Estimation of Signal Parameters using Rotational Invariance Technique) is an estimation technique that makes use of the rotational properties of the frequency matrix in order to find a way to estimate those frequencies.

The data matrix, $\mathbf{X}$ shown above can be expressed as;

$\mathbf{X} = \mathbf{A} \cdot \mathbf{S}$, where: $\mathbf{S} = \begin{bmatrix} \beta_1 & \beta_1 e^{j\omega_1} & \cdots & \beta_1 e^{j(N-m+1)\omega_1} \\ \vdots & \vdots & \ddots & \vdots \\ \beta_n & \beta_n e^{j\omega_n} & \cdots & \beta_n e^{j(N-m+1)\omega_n} \end{bmatrix}$

If an SVD of data matrix $\mathbf{X}$ is formed such that: $\mathbf{X} = \mathbf{U}\mathbf{\Sigma}\mathbf{V}^H$; it can be shown that, there is a non-singular matrix $\mathbf{C}$ such that, $\mathbf{U} = \mathbf{A}\mathbf{C}$.

Let's form matrix $\mathbf{U}_1$ and $\mathbf{U}_2$ such that: $\mathbf{U}_1 = [\mathbf{I}_{m-1}\, 0]\mathbf{U}$ and $\mathbf{U}_2 = [0\, \mathbf{I}_{m-1}]\mathbf{U}$ and matrix $\mathbf{A}_1$ and $\mathbf{A}_2$ such that: $\mathbf{A}_1 = [\mathbf{I}_{m-1}\, 0]\mathbf{A}$ and $\mathbf{A}_2 = [0\, \mathbf{I}_{m-1}]\mathbf{A} = \mathbf{A}_1\mathbf{T}$, where $\mathbf{T} = \begin{bmatrix} e^{j\omega_1} & & 0 \\ & \ddots & \\ 0 & & e^{j\omega_n} \end{bmatrix}$.

This implies that:$\mathbf{U}_1 = \mathbf{A}_1\mathbf{C}$ and $\mathbf{U}_2 = \mathbf{A}_2\mathbf{C}$. Hence,

$$\mathbf{U}_1^{\dagger}\mathbf{U}_2 = \mathbf{C}^{-1}\mathbf{T}\mathbf{C}$$

This implies that the matrix $\mathbf{T}$, hence the frequencies on its diagonal, can be estimated by eigen value decomposition of the matrix: $\mathbf{U}_1^{\dagger}\mathbf{U}_2$ [24].

The matrix containing the amplitudes, $\mathbf{S}$ can be obtained as:$S = \mathbf{C}\mathbf{U}^H\mathbf{Z}$. Then, $|\mathbf{S}|$ contains $N - m + 1$ columns consisting of the same estimate $[\beta_1, \beta_2, \cdots, \beta_n]^T$. Hence, the final estimate of the amplitudes can be made by averaging over the columns of $\mathbf{S}$.

4.4 Joint Time-Frequency Processing

In Chapter 2, Section 2.1, it is discussed that the human motion can be conveniently represented in the velocity versus time plot. It is shown that the human motion velocity profile consists of different velocity components each having different magnitudes and these velocity components change fast through time as shown in Figure 2.1. The same applies to the frequency content of the Doppler signal.

Let's take the received data of length N modeled above. To estimate the Doppler velocity components from this signal, the spectral estimators use the assumption that the signal of length N is stationary. For instance, the DFT of the signal y_n is given by,

$$Y[k] = \sum_{n=0}^{N-1} y[n]\, e^{-j2\pi nk/N}$$

where $k = 0, 1, ..., N-1$. However, human motion is non-stationary by nature. Hence, the Doppler signal, y_n is also non-stationary. This makes the DFT by itself not useful to see the frequency content of the signal.

The way to analyze such a signal is therefore to view the change both in time and frequency domains. That is to estimate the frequency components of the Doppler signal of a short time window and to view the variability of these frequency estimates as a function of time. Such a joint way of characterizing the time-varying frequency content of the signal in both time and frequency domain is called joint time-frequency processing.

4.4.1 Short time Fourier transform (STFT)

A person walking in an indoor environment is in a non-uniform motion; however the person's velocity can be assumed to remain constant during short time intervals, i.e., physical constraints will limit the person from changing his velocity during short time intervals. Thus, a non-uniform human motion can be viewed as a uniform motion over small time or displacement intervals. This implies that, even though the received signal, y_n is non-stationary it can be assumed as a piece-wise stationary signal.

The discrete Fourier transform of a signal defined based on this piece-wise assumption is called short time Fourier transform (STFT) and it is given by,

$$Y\left[k, n'\right] = \sum_{n=-\infty}^{\infty} y\left[n\right] w\left[n' - n\right] e^{-j2\pi nk/N_{fft}} \tag{4.3}$$

n is a local time index describing the sequence y_n, the windowing time index (refered simply as 'time index' from now on) is labeled n' to distinguish it from the local time index, $k\{0, 1, \cdots, N_{fft}\}$ is the frequency index, N_{fft} is the size of the FFT required and $w\left[n' - n\right]$ is a sliding window function. The STFT is thus the DFT of a weighted segment of the input signal.

The time index at which the spectrum is calculated, n' is the center of the windowed segment of the signal. n' can be expressed in terms of the window length, L and the percentage of overlap, x required between consecutive windows. That is, n' is equal to the integer value of $L(0.5 + i(1 - x))$, where $i = 0, 1, 2, \cdots$. Hence, the time interval between consecutive frequency estimations is equal to,

$$\Delta n' = (1 - x)L \tag{4.4}$$

Window Size:

The length of the window, L is a trade off between spectral resolution, which is equal to $\frac{1}{L}$, and the risk of non-stationarity. A longer window size gives a better frequency resolution and has a lower statistical variance (better accuracy). On the other hand, a shorter window size provides better time resolution and satisfies the piece-wise stationarity assumption used in STFT. Thus, time-frequency resolution is a trade-off in STFT. Hence, considering these factors, the following parameters are used in the STFT based on the requirements in Section 3.3.

- Sampling frequency, f_s of $500S/sec$ is used as stated in the requirements.

- L should be short enough such that the stationarity requirement is fulfilled. That is a time resolution of $0.2sec$ (a window seize of $L = 100$ *samples*) is used in the STFT.
- This gives a frequency resolution of $\frac{1}{0.2sec} = 5Hz$ in non-parametric frequency estimators; this resolution is worse than the frequency resolution requirement of $1Hz$.

Window Type:

The type of window is also a trade-off like the window size. On one hand, the main lobe width of a windowing functions cause smearing (low resolution). On the other hand, using smooth windows reduce leakage (variance of the spectral estimate). A rectangular window provides the best resolution; however it has a higher leakage than the other windows. Other windows have low side lobe levels and hence low leakage; however, the main lobe of other windows such as Bartlett, Hamming, Hanning, Blackman, Kaiser, etc., is wide and hence has smearing (smoothing) effect.

For human movement characterization applications, a high resolution is required to avoid the smearing of the reflection from the different body parts. On the other hand, less leakage is required so that the RCS (power) from each component is not overestimated due to leakage. Moreover, the velocity bandwidth can be overestimated due to leakage of the window used. Thus, in extraction of some parameters, discussed in Chapter 5, resolution may be more important and for other parameters avoiding leakage is important. So, a window type will be selected accordingly.

However, the Hamming window which is shown in Figure 4.2 is selected in all other cases that require an optimal balance between leakage and resolution.

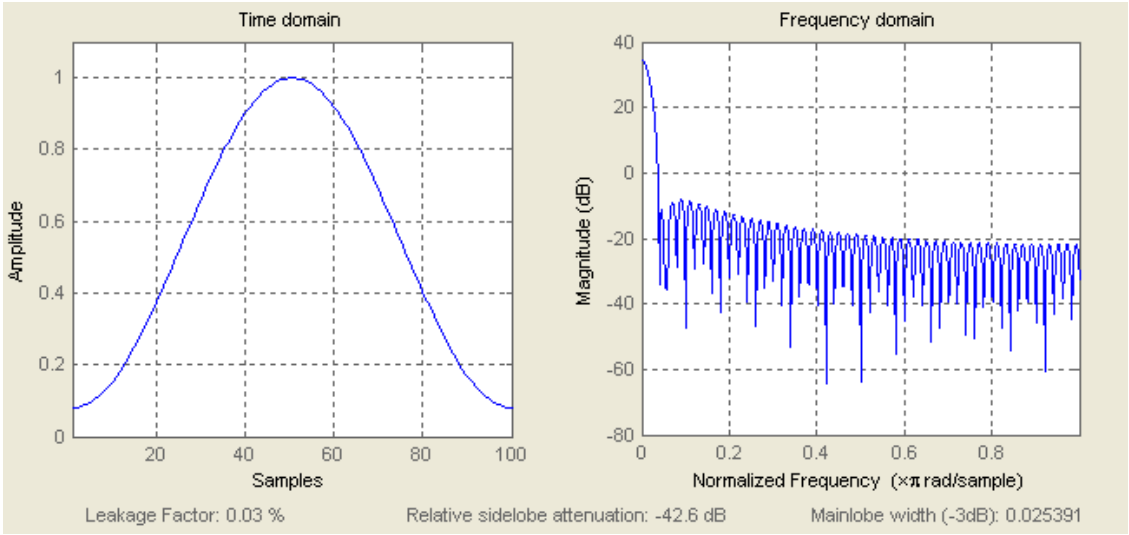

Figure 4.2: Hamming Window

Zero Padding and Overlap:

As discussed above, time resolution is dependent on the window size, L and the frequency resolution of STFT is proportional to $1/L$. However, zero padding in the time domain can be used to get a smooth spectrum in the frequency domain. Equivalently, higher overlap between STFT windows in the time domain can be used to obtain a smooth STFT plot in the time axes. Thus, zero padding and overlap do not add information to the time-frequency estimation.

In (4.3), padding the data of size, L with zeros to a size $N_{fft} > L$ will not change the frequency resolution; however will increase the number of frequency points leading to a smooth plot in the frequency domain. Similarly, increasing the overlap, x in (4.4) decreases the distance, $\Delta n'$ between time points; thus, it results in a smoother plot in the time domain. The only problem of increasing these parameters is the high computational complexity. In the STFT analysis, the following values are selected;

- Size of FFT: The size of FFT is set such that the frequency resolution, $\frac{fs}{N_{fft}}$ satisfies the requirement, $1Hz$. Thus, $N_{fft} = fs = 500$ is selected.
- Overlap: An overlap higher than 0.75 can cause to much complexity. Thus, a rough selection of $x = 0.75$ (75% overlap) is selected.

4.4.2 Spectrogram

The spectrogram is a plot of the magnitude of frequency components versus time in a joint time-frequency estimation. The pixels in a spectrogram can be obtained using the discrete STFT and are represented by: $P[k, n']$, where $P[k, n'] = |Y[k, n']|^2$ or in logarithmic scale, $P[k, n']_{dB} = 10 \cdot \log |Y[k, n']|^2$.

Each pixel in the spectrogram shows the power of the k^{th} frequency component of the signal at time instant, n'. Hence, the whole spectrogram shows the frequency components of the signal, the power content of these frequencies and how the power content changes through time. Whenever, the phase of the frequency estimate is also required, the spectrogram estimate $P[k, n']$ can be represented as, $P[k, n'] = |Y[k, n']|^2 . e^{j(angle(Y[k,n']))}$.

4.4.3 Sliding Window Parametric Estimators

The major problem with the STFT is that the time and frequency resolution are dependent on the window size in an inverse manner. That is, there will be low time resolution if there is good frequency resolution and vice versa. To solve this problem wavelet transform could be one approach. However, the multi-resolution nature of wavelets has a limitation by itself. The scaling is such that there is a high frequency resolution and a low time resolution at low frequencies and vice versa at high frequencies. However, it is difficult to assume that natural phenomena including Doppler signals require this type of resolution. Thus, the best way to estimate the spectral content of Doppler signals with good time-frequency resolution is to use signal dependent estimators, i.e., to use sliding window parametric estimators.

The way to apply the sliding window to the parametric estimators is the same as the STFT. In addition, the spectrogram[3] from MUSIC describing the magnitudes is computed similarly.

- The signal is decimated to a sampling rate of $f_s = 1000 samples/sec$, twice the sampling frequency used for the non-parametric case; because, having more points affects the estimation accuracy of parametric estimators.
- A window of size $L = 0.2sec$ is used.
- A rectangular window is used as there is no need to use other window functions for parametric estimators.
- The statistical accuracy of MUSIC increases with increasing m (the number of columns in the data matrix); however, so does the computational complexity. m should be much less than N to have better estimation of the covariance matrix. In addition, m must be greater than D (the number of sinusoids), i.e., $D < m < N$. Hence, $m = N/2$ is selected as an optimal value assuming the number of sinusoids, D is less than $N/2$.
- The eigen-based methods have high resolution in general. Thus, the MUSIC cost function is sampled at $1Hz$ frequency resolution so that the requirement of Section 3.3 is satisfied.

Estimation of Number of Sinusoids, D

One of the major parameters that should be known for parametric spectral estimation is the number of sinusoids, i.e., the parameter, D in (4.2). Moreover, the number of sinusoids is different from window to window as the human motion is not uniform.

The parameter, D can be estimated from the singular value decomposition of the data matrix $\mathbf{X}$ and an assumption on the maximum number of frequency components expected in a static (no motion) condition, D_{sta}. This parameter is not easy to set; however, the number of maxima greater than a threshold value can be taken for instance as a measure of D_{sta} . For instance, considering the clutter spectrum in Figure 4.3; the number of maxima greater than $65dB$ can be taken as 7; thus, this value can set as D_{sta}.

The singular values, σ_i of the data matrix $\mathbf{X}$ in a sliding window, $\mathbf{X}_{win} = \mathbf{U\Sigma V}^H$ will consist of D singular values of the signal and $m - D$ singular values of the noise. So, each singular value σ_i is compared to the $(D_{sta})^{th}$ singular value of the data matrix at static condition. Thus, the value of D in a given window is the dimension at which $\sigma_i \leq$ the $(D_{sta})^{th}$ singular value. Hence, different value of D can be used in each time window.

As already discussed $D = M \cdot R$ where M is the number of body parts and R is the number of signal paths in the indoor environment. The estimated value of D can thus

[3]The spectrum from MUSIC is a pseudo-spectrum; however this spectrogram still shows at which frequencies the signal has stronger spectral content and at which frequencies it is weaker. Thus, MUSIC can also be used as power spectral density estimator.

be compared to the approximate number of sinusoidal components expected from human motion.

What should be considered carefully is that underestimating D, is equivalent to taking the actual sinusoidal components as white noise which makes the parametric estimations inaccurate in distinguishing the signal and the noise singular values. So, the value of D should be taken large enough so that the remaining noise component can be assumed as white noise. Even though, the number of sinusoids is different from window to window; it is better to take the same D for all windows. Thus, the value of D from each estimation window is computed and the highest value, D_{max} is used as the number of sinusoids, D in all windows.

4.5 Background Spectrum Subtraction

The signal received by a radar receiver consists of a strong direct signal from the Tx to the Rx. There is also a clutter reflected from stationary objects such as walls in an indoor environment. In addition, there are some spurious signals that always occur at some frequencies around the carrier frequency due to the receiver characteristics and frequency response of the antenna used as the background noise spectrum in Figure 4.3 shows. Thus, background subtraction is essential in order to reduce these background signals, so that the frequency components due to the motion become evident.

Spectral subtraction methods are common in speech processing. Noise can be suppressed from speech using spectral estimation by estimating the noise during a non-speech interval [25], [26]. The same analogy can be used in radar signal processing. By estimating the noise when the environment is static (when there is no motion), the background noise spectrum can be estimated. Then, spectral subtraction can be done based on the estimated background signal.

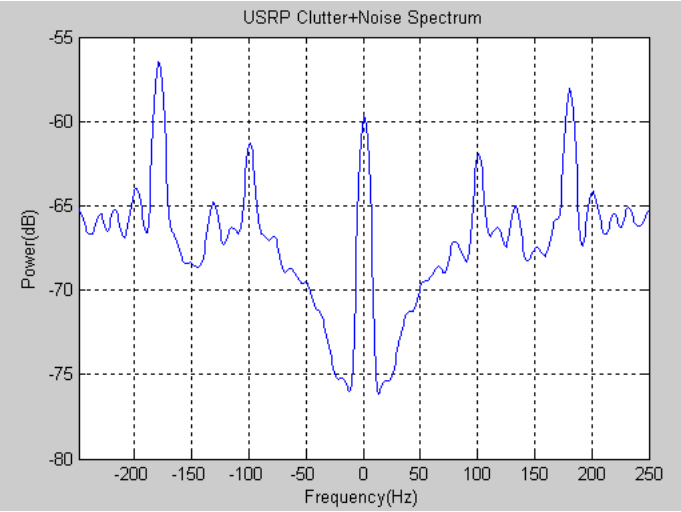

Figure 4.3: Background signal spectrum

Let's consider the noisy spectrogram pixel estimate at frequency index, k and time index, n' : $P[k, n']$. This estimate consists of background noise, $P_{back}[k, n']$ and the actual signal due to motion, $P_m[k, n']$. That is $P[k, n'] = P_m[k, n'] + P_{back}[k, n']$. Thus, the expected value of the background noise can be subtracted from each computed pixel, $P[k, n']$ in order to obtain $P_m[k, n']$. That is, $\hat{P_m}[k, n'] = P[k, n'] - P_{back}[k, n']$.

The expected value of the background signal at each frequency, $P_{back}[k]$ can be used instead of $P_{back}[k, n']$and it can be estimated by averaging over the time index, n'. That is $P_{back}[k] = E\left\{|P_{back}[k, n']|^2\right\} \approx \frac{1}{N}\sum_{n'=1}^{N}|Y_{back}[k, n']|^2$. Thus, the power of the Doppler signal due to motion only, $\hat{P_m}[k, n']$ can be estimated as:

$$\hat{P_m}\left[k, n'\right] = P\left[k, n'\right] - P_{back}[k] \tag{4.5}$$

What if the magnitude $P[k, n']$ is less than $P_{back}[k]$? In that case, $\hat{P_m}[k, n']$ must be set to the spectral floor. Therefore, a general expression is defined using flexible constants α, β and γ [26] such that:

$$\hat{P_m}^{\gamma}\left[k, n'\right] = \begin{cases} P^{\gamma}[k, n'] - \alpha P_{back}^{\gamma}[k] & \text{, if } P[k, n'] > (\alpha + \beta)P_{back}[k] \\ \beta P_{back}^{\gamma}[k] & \text{, otherwise} \end{cases} \tag{4.6}$$

β sets the spectral floor and α is a subtraction parameter used as a correction factor for the underestimated expected value of the noise. The power index, γ gives the option for power or magnitude subtraction; $\gamma = 1$ is for power subtraction and $\gamma = 0$ for magnitude subtraction. The spectral floor can be set uniformly to βP_{bm}^{γ} instead of the frequency dependent $\beta P_{back}^{\gamma}[k]$, where P_{bm} is the minimum value of $P_{back}[k]$. This is to make the spectrum in a static condition frequency independent. There is no need of using a scaled down colored noise again; rather, it is better to make the noise partly white.

In order to create a smooth spectrogram that avoids spectral deeps and peaks, $\alpha > 1$ and $\beta > 0$ should be selected. The other reason to set $\alpha > 1$ is the spectral leakage that results from the spectral estimators. That is, a frequency component with no Doppler signal component will have a higher magnitude during motion than static condition due to spectral leakage. Thus, setting higher α increases the threshold $(\alpha + \beta)P_{back}[k]$ so that such leakage is treated as noise. The value of β depends on the spectral peaks and valleys expected.

Basically there are two ways to make the spectral subtraction. Either of these methods could be suitable in different scenarios based on which signal parameter is to be extracted.

1. Subtraction in the spectrogram: This is pixel based subtraction on the spectrogram as shown above using (4.6). In this subtraction, γ is set to 1 ; since, power subtraction is more suitable for the visual spectrogram. An example of this spectral subtraction is shown in Figure 4.4 for $\alpha = 3$, $\beta = 0$ and $\gamma = 1$.

2. Subtraction in time domain: After spectrogram subtraction in (1) , then the subtracted signal is taken as the phase of the original signal, i.e., $\hat{P_m}[k, n'] = P_m[k, n'] \cdot e^{j(angle\, P[k,n'])}$. Windowed IFFT is then applied to get a time domain

signal free of the background signal. $\alpha = 3$, $\beta = 0.1$ and $\gamma = 0.5$ are selected here as magnitude subtraction is more suitable to transform the signal back to time domain. This subtraction method is used in displacement estimation.

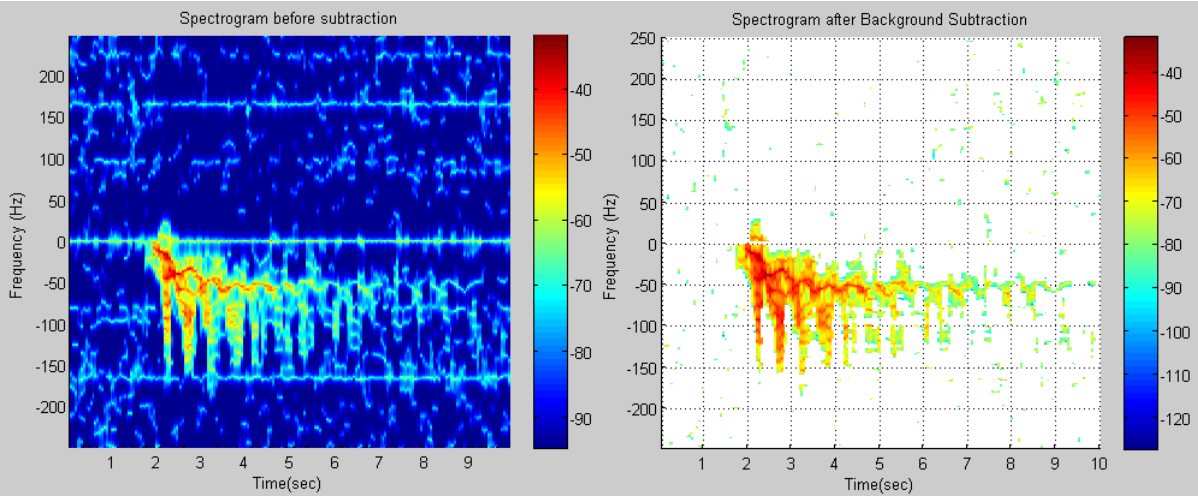

Figure 4.4: Spectrogram before and after background subtraction

4.6 Quadrature Demodulation

It is discussed in Chapter 3 that the signal received from a target after transmitting CW signal is phase modulated with the motion pattern. The Doppler signal model can be expressed in terms of the change in phase from sample to sample as:

$$y[n] = \sum_{k=1}^{D} \left[a_k[n] \cdot e^{j(\Delta\phi_k[n] + \phi_k[n-1])} \right] \tag{4.7}$$

where $D = M \cdot R$ is the number of path of the signal, $a_k[n]$ is the amplitude of each path k at time instant n, $\phi_k[n-1]$ represents the phase at time instant, $n-1$ and $\Delta\phi_k[n] = \phi_k[n] - \phi_k[n-1]$. Assume that the remaining noise component is white.

Let's make a rough assumption that the number of strong paths, D is only two: a direct path (which contains no Doppler information) and one multipath ray reflected off the person. In that case the signal model will reduce to a very simple expression:

$$y[n] = a_1[n] + a_2[n] \cdot e^{j(\Delta\phi[n] + \phi[n-1])} \tag{4.8}$$

The direct path amplitude, $a_1[n]$ can be removed after estimation by windowed averaging of the input signal. Thus, the change in phase between samples, $y[n]$ and $y[n-1]$ can be estimated using Quadrature demodulation ,

$$\Delta\phi[n] = arctan((y[n] - a_1[n]) \cdot (y[n-1] - a_1[n-1])^*)$$

The total change in phase with respect to the initial point where motion starts, $\Delta\phi_T[n]$ can thus be calculated as,

$$\Delta\phi_T[n] = \sum_{i=1}^{n} \Delta\phi[i] \tag{4.9}$$

The assumption here is that this change in phase is caused by motion of the human target only. Thus, the radial displacement can be estimated based on this change in phase. The major problem with this change in phase, $\Delta\phi_T[n]$ is when the noise or clutter spectrum is not white as shown in Figure 4.3. In that case, the background spectrum subtraction in time domain discussed in Section 4.5 can be used.

Chapter 5

Parameter Extraction

As already introduced in Chapter 2, there are different parameters of human motion that characterize human activity and that can be obtained from the velocity profile. When using radar for human activity characterization, the body velocity profile is obtained in terms of Doppler frequency profile. Thus, the parameters of human motion are extracted based on time-frequency estimation of the Doppler signal.

The variation of the received power of the Doppler signal is used for quantifying activity, i.e., to compute the activity index. The change in the phase of the signal estimated using quadrature demodulation gives another important parameter that quantifies activity, i.e., the displacement of the person. On the other hand, applying different techniques on the spectrogram estimated in Chapter 4 will enable the estimation of different movement parameters such as torso velocity, cadence frequency, step length, velocity bandwidth, etc. Estimation of these parameters from the received signal can make automatic human movement identification and classification possible by training the classifiers. In this Chapter, the methods used to estimate the movement parameters for human activity quantification, identification and classification are discussed.

The spectrogram is described by time index, n', frequency index, k and the power at each pixel: $P[k, n']$. Thus, at each time index, n' angular frequencies $[\omega_1, \omega_2, \cdots, \omega_D]$ are obtained which constitute the angular frequency range $[-\pi : \pi]$. From now on, frequency, $f_k = \frac{\omega_k}{2\pi}$ is used to denote each Doppler frequency instead of ω_k and k_{max} denotes the frequency index for ω_D.

5.1 Parameters to Quantify Activity

5.1.1 Activity Index

One of the ways to define an index that varies in proportion to the level of movement, activity index is using the variation in the power of the channel. This definition is based on two assumptions:

- The quantity of activity is proportional to the change in position of the person.

- The only factor that causes time variation of the received CW signal power is human activity.

Thus, the activity index (AI) at a particular time can be related to the standard deviation of the power windowed around that time instant. However, the AI estimated using standard deviation will depend on the distance of the human target from the radar. To avoid this dependency, the standard deviation is normalized by the average value of the signal at a particular window. This is based on the assumption that the mean signal power is much higher than zero. The activity index changes over time; thus, the index should be calculated over windowed versions of the signal. Thus, a rectangular sliding window is used to calculate a moving standard deviation to mean ratio. The window size, L is set to $1sec$; since the power does not vary too often as compared to the micro-Doppler pattern which requires a window of size, $0.2sec$.

The standard deviation of the power of the signal is calculated using a sliding window to get the activity index, $AI\left[n'\right]$. That is,

$$AI\left[n'\right] = \frac{\sqrt{\frac{1}{L}\left(\sum_{n=-\infty}^{\infty}\left(P\left[n\right]\cdot w\left[n'-n\right]\right)^2\right) - \left(\frac{1}{L}\sum_{n=-\infty}^{\infty}P\left[n\right]\cdot w\left[n'-n\right]\right)^2}}{\frac{1}{L}\sum_{n=-\infty}^{\infty}P\left[n\right]\cdot w\left[n'-n\right]}$$

where, n' is the time index, n is the local time index, $P\left[n\right] = \left|y\left[n\right]\right|^2$ is the power of each sample, and $w\left[n'-n\right]$ is a rectangular window of size L.

Then, the activity index can be normalized to the maximum value over a certain time duration in order to get an activity index in the interval $[0:1]$.

5.1.2 Displacement versus Time

The other parameter that can quantify overall activity in an indoor environment is the total displacement of a person with respect to the origin of motion. The displacement estimated from radar data is the radial component of the actual displacement of the person. This radial displacement can be obtained in two ways:

- Displacement can be obtained from the phase variation obtained from quadrature demodulation in (4.9). The total displacement, Δx_T can be calculated as: $\Delta x_T = \lambda\frac{\Delta\phi_T}{4\pi}$. The displacement,$\Delta x_T$ may be overestimated in a static condition due to colored background noise spectrum. Thus, the time domain background spectrum subtraction technique discussed in Section 4.5 is applied before using this algorithm.

- Displacement is also equal to the area under the torso velocity vs time curve. Thus, after estimating the torso velocity from the spectrogram (Section 5.2), the total displacement can be calculated.

5.1.3 Direction of Motion

Direction of motion is one of the important parameters of human movement. When combined with other parameters it can give an idea of the position of the person and where in the room the person is heading to at a particular time. As already described in Chapter 3 :

- Approaching targets increase the frequency of the RF signal; hence result in a positive Doppler shift.
- Receding (moving away) targets decrease the RF frequency; hence result in a negative Doppler shift.

Therefore, the position of the strongest frequencies in the frequency domain shows the direction the object is moving. In addition, the change in direction of motion can be seen from the spectrogram. For automatic direction identification, the sign of the difference of the sum of powers at Doppler frequencies, $f_k > 0$ and $f_k < 0$ can also be taken in each time window to determine the direction of motion for automatic identification, i.e.,

$$Direction\left[n'\right] = sign\left\{\sum_{f_k=0}^{fs/2} P\left[k,n'\right] - \sum_{f_k=-fs/2}^{0} P\left[k,n'\right]\right\}$$

5.2 Identification Parameters

The parameters to identify human movement from non-human movements are introduced in Section 2.2.1. These parameters are estimated as follows:

1. ***Torso velocity***, $v_{torso}\left[n'\right]$: The instantaneous torso velocity is expressed in terms of the torso frequency as: $v_{torso}\left[n'\right] = \frac{2\pi}{\lambda} f_{torso}\left[n'\right]$. The torso frequency can be obtained in two ways:

   (a) Selecting the frequency of maximum power from each column in a spectrogram, i.e., $f_{torso}[n'] = f[k_{torso}, n']$, where, k_{torso} is the frequency index at which $P\left[k,n'\right]$ is maximum. The torso velocity is set to this value if there is motion otherwise the torso velocity is set to 0. Doppler signal detection can be made by calculating the standard deviation of $P\left[k,n'\right]$ at each time index, n' and comparing it with a threshold. The threshold can be set based on the standard deviation of the background signal, $P_{back}[k]$ in Section 4.5. Power at $f_k = 0$ can be removed by averaging the signal or using background subtraction.

   (b) Weighted velocity estimation in each column, i.e.,

$$f_{torso}\left[n'\right] = \frac{\sum_k f\left[k,n'\right] \cdot P\left[k,n'\right]}{\sum_k P\left[k,n'\right]}$$

The former method is generally a better estimator than the latter; because, the latter gives a biased estimate due to image frequencies (in multipath environment) and due to oscillations of the appendages. However, the latter method performs well even in static conditions; in addition, it is more easier to apply as there is no need for threshold.

2. ***Cadence frequency***, f_c: Cadence frequency is obtained by taking the FFT of the spectrogram in the horizontal direction at each Doppler frequency. Thus, the Doppler frequency versus time plot will be transformed into Doppler frequency versus cadence frequency plot.i.e.,

$$P_c\left[k,c\right] = \sum_{n'=1}^{N_W} Y\left[k,n'\right] e^{-j\left(\frac{2\pi}{N_W}\cdot c\cdot n'\right)}$$

where $P_c\left[k,c\right]$ is the power at Doppler frequency index k and cadence frequency index c . The number of windows involved in the FFT, N_w should be short enough to estimate the changing cadence frequency; however, it should be long enough to get sufficient cadence frequency resolution. Thus, an optimal number of windows should be taken considering these factors. The maximum cadence frequency depends on the sampling time in the spectrogram, i.e., the time interval between consecutive windows shown in (4.4).
In order to obtain the cadence frequency of the gait, the total power of the signal at each cadence frequency is computed by summing over the Doppler frequency bins. Thus, sum of the power over the Doppler bins gives a magnitude versus cadence frequency plot. However, the sum should be computed over $f_k > 0$ or $f_k < 0$ depending on the direction of motion. This is to avoid the effect of the image frequencies in indoor environment. Thus, the cadence magnitude, $P_c\left[c\right]$ is computed as: $P_c[c] = \sum_{f_k=0}^{f_D} P_c[k,c]$. Based on the velocity profile model in (2.1), three peaks are expected in the cadence frequency curve at frequencies of 0, ω_c and $2\omega_c$. Thus, the second peak from the cadence frequency plot is taken as the fundamental cadence of the gait.

3. ***Step length***, S_l: Step length is obtained from the fundamental cadence frequency, f_c and the torso velocity, v_{torso} using the expression: $S_l = \frac{v_{torso}}{f_c}$.

5.3 Classification Parameters

Parameters to classify human activity into a certain group of activities such as walking, jogging, exercising, crawling, sitting with slight arm movement, etc., are already discussed in Section 2.2.2. These parameters can be obtained from the spectrogram as follows:

1. ***Torso velocity*** *&* ***cadence frequency***: already discussed above in Section 5.2.

2. ***Velocity Bandwidth***: In order to obtain the velocity bandwidth, the upper and lower frequency envelopes of the micro-Doppler pattern should be estimated. The

envelope estimation will be more accurate if frequency leakage in the spectral estimation is minimized. These envelopes consist of a set of frequencies at which the maximum and the minimum micro-Doppler frequencies exist in each time window. Let's assume that these upper and lower envelopes at time index n' are represented by, $f_{UE}[n']$ and $f_{LE}[n']$ respectively. In order to estimate this envelopes:

- A threshold is set in order to distinguish the micro-Doppler pattern from noise or background signal and hence to estimate the envelopes.
- The Spectrogram is scanned from $k = 1$ to $k = k_{max}$ for $f_{LE}[n']$ and $k = k_{max}$ to $k = 1$ for $f_{UE}[n']$ until micro-Doppler pattern is detected.
- ***Threshold level***: The threshold should be frequency dependent as the background noise is frequency dependent by itself. Therefore, a background noise, $P_{back}[k]$ as discussed in Section 4.5 is calculated; then it is multiplied by a factor, α to account for the frequency leakage due to the spectral estimators. Thus, the threshold at frequency index, k is set to $\alpha \cdot P_{back}[k]$. In order to minimize false detection due to frequency leakage, an α value as large as $20(13dB)$ is used.

3. ***Standard Deviation***: The other parameter that is important is the power distribution over the velocities within the velocity envelope. Thus, the standard deviation can be computed to see the extent to which the power distribution varies over the velocities in the envelope.

5.4 Velocity Profile

It is discussed in Chapter 2 that the velocity profile is the major characteristics of human motion. Accurate estimation of this profile enables identification and classification of human activity. Moreover, accurate estimation of this parameter will be one step towards identifying a person by his gait pattern. Thus, it would be very beneficial if the velocity profile shown in Figure 2.1 can be obtained from radar data. One possible attempt to obtain of this profile is described as follows.

Let's assume that we need to obtain the velocity profile from the 12 significant and rigid parts of the body. Thus, 12 significant frequencies should be extracted in each time index, n' for each body part. This can be done in two ways;

- The MUSIC spectrogram is estimated and the local maxima are extracted from it based on a threshold value. Then, the largest12 maxima are taken in each time index.

- The spectrogram is computed using sliding window ESPRIT. The highest 12 power values and the corresponding frequencies are selected and the points are arranged in order of increasing frequency. However, the problem of this method is that the frequencies estimated might be frequencies of the highest power component only rather than local maxima.

Then, the next step is joining a frequency index in a window, n' to its corresponding index in the consecutive window, $n' + \Delta n'$. For instance, the power and frequency from the leg in one window should be matched to the corresponding values in the next window in order to obtain sets of points which describe the velocity profile of the leg. Thus, a certain tracking criterion should be used to track the frequency from each body part through time. One criterion that can be used is the assumption that contribution of each body part to the RCS (hence the power) remains constant through time. Thus, the body part with the highest power component in one window should remain being the highest in the consecutive windows and the 2nd highest will remain the 2nd highest, etc. These frequencies which correspond to the descending order of powers in each window can be thus tracked.

Now, points of the velocity profile of each body part, $v_m[n']$ given in (2.1) are estimated. The velocity of the body, V and the cadence of the gait, ω_c in (2.1) are already estimated in Section 5.2. Now, the remaining parameters are the amplitudes of oscillation. Thus, can we apply some parameter estimation techniques to come up with the amplitude parameters of the velocity profile: $k_{m1}, k_{m2}, k_{m3}, k_{m4}$?

Chapter 6

The Experimental Platform

The goal of this thesis is not only to extract parameters that characterize human movement; but also to use a low-cost, flexible transceiver as a radar.

In this Chapter, the overall hardware and software architecture of the radar platform used in this thesis is described. Then, the limitations of this platform for the purpose of measuring human movement Doppler shift are discussed. The limitations of the platform lead to the discussion on which radar type can be implemented using this platform. It is discussed why the CW radar is the radar type selected to be implemented on this platform. The Chapter is concluded by discussing the major advantages of a GNU Radio based radar in general.

6.1 Software Defined Radio

Software defined Radio (SDR) is any radio system that performs modulation and demodulation of a signal in software. The extent to which a system should consist of a software part in order to be categorized as an SDR is not clearly defined. However, the general philosophy of SDR is keeping the software as close to the antenna as possible.

SDR tries to translate the radio engineering problem from the hardware to the software domain. The major advantages of this translation include:

- ***High flexibility***: Using SDR gives the flexibility to adapt to new services and standards. Any processing that can be done in hardware can be done in software with better flexibility. SDR can be modified or upgraded by modifying software blocks which makes it flexible as compared to changing hardware components in hardware systems.

- ***General purpose hardware***: A single hardware can be used for different radio systems just by modifying the software block attached to the general purpose hardware.

- ***Predictability***: SDR has predictable and repeatable results as compared to hardware radios.

- ***Easy access***: It is easier and convenient to access and view a signal between signal processing blocks as compared to a signal between hardware components.

However, the extent to which the software in communication or radar systems can be pushed closer to the antenna is limited. Some of the factors that lead to these limitations include:

- ***Sampling rate of ADC***: The sampling rate of the ADC should be twice the maximum frequency in the signal of interest based on the Nyquist theorem[1]. For most radio applications, the signal is modulated on carriers of many GHz; however, ADCs of such high sampling rate are rare and costly. Thus, hardware front-ends are required to bring the signal down to a lower frequency.

- ***Processing speed***: Again, to realize such SDR systems the processor should be able to process the signal sampled at high sampling rate in real time. This is not possible with the currently existing general purpose processors.

The most common currently realizable SDR uses high speed ADC. Then, high speed software processing is done on FPGA (Field programmable gate arrays) to lessen the computational burden of the host processor and to avoid port/bus bandwidth bottlenecks.

6.2 Platform Overall Architecture

The radar platform used in this thesis is a software defined radio that consists of a USRP as hardware platform and a GNU Radio as software platform. The combination of these two provides the necessary flexibility required for building a radar system that can transmit various types of waveforms (with some limitations) and receives the corresponding reflection or echo from the target using the same hardware.

The USRP and GNU Radio combination is currently being used in various communication systems as cognitive radio front end, GPS receiver, IEEE 802.11 node, GSM node, FM/AM transceiver etc. Moreover, there is a research on using this platform as passive presence detection radar, by sensing the variation of GSM signals.

The overall block diagram of transmission and reception involving the USRP and the GNU Radio is shown in Figure 6.1. As the figure shows, the radar consists of a USRP, GNU Radio and daughter boards which consist of the RF front-end. This GNU Radio based radar works as follows:

Sequence of bits to be transmitted is coded and modulated in the general purpose computer and sent to the FPGA. In the FPGA, the discrete data is interpolated and up converted to an IF frequency. Then, the signal is converted to analog by the ADC and modulated to RF frequency by the RF front-end before transmission. The signal reflected off the target is received by the Rx antenna, and then filtered and down converted to

[1]The Nyquist criterion states that exact reconstruction of a continuous time signal is possible if the signal is band-limited and if the sampling frequency is greater than twice the maximum frequency content of the signal.

an IF frequency. The IF signal is then sampled by the DAC, further down converted and decimated by the FPGA. Finally, the low rate data is sent to the general purpose processor for demodulation,decoding and further analysis.

A detailed description of the parts of the platform including the USRP, GNU Radio and daughter boards is found Appendix A and B.

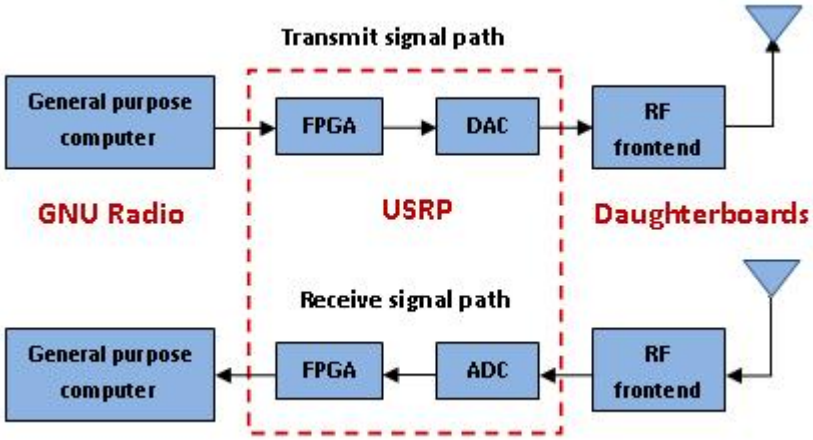

Figure 6.1: GNU Radio based Radar Block Diagram

6.3 Limitations of the Experimental Platform

The hardware platform discussed in Appendix A can be used as a radar for characterizing human activity. However, the platform has some limitations that require further analysis in order to come up with the ways and modifications necessary to use it for the application concerned.

6.3.1 Isolation in the USRP

As described in Appendix A, the USRP can work as a transceiver. However, this is true provided the necessary isolation is maintained between Tx and Rx circuits in terms of frequency, space or time. In our radar, the transmitted and received signals are not separated in frequency as the Doppler frequency of the target is too small as compared to the carrier. There is no separation in time as it is a short range application which requires simultaneous transmission and reception. Thus, here is the effect when there is little space isolation as it is the case when one USRP is used as transceiver radar.

According to the USRP designers, there is no more than $20dB$ isolation between the Tx and Rx circuits on a single USRP. Since the dynamic range of the USRP ADC is $74dB$[2], the minimum ratio of received echo to transmitted signal, $\frac{Pr}{Pt}$ that can be distinguished becomes $-94dB$. This means if dipole antennas are used in a monostatic

[2]Dynamic range of N-bit ADC=6.021·N +1.763 and N=12 for the USRP ADC.

scenario, the maximum distance from which the echo can be distinguished will be, $10m$ based on (3.8). This is a very optimistic result with ideal assumptions including the assumption that the full dynamic range of the ADC is being used. In actual conditions, the sensitivity distance is much shorter (this is also verified by experiment). Thus, it is concluded that a single USRP does not provide the necessary isolation required to distinguish an echo from farther distance.

Therefore, two USRPs with two daughter boards are used in our validation experiments as shown in Figure 7.1 in order to avoid these isolation problems.

6.3.2 Phase Noise & Frequency offset

Using two USRPs solves the isolation problem; however, two big problems arise in the platform: variable frequency offset and phase noise. This is because the daughter boards use a phase locked loop based frequency synthesizer with a reference clock from the USRP as discussed in Appendix A.2. In this case the reference clocks are taken from two different motherboards each consisting $64MHz$, $20ppm$ clocks. Thus, the daughter boards are set to clocks of different frequencies and phase thus causing the variable offset and phase noise. This makes extraction of very low Doppler frequencies around the carrier impossible.

The phase noise and variable frequency offset when using two USRPs and is shown in the time-frequency plot in Figure 6.2. Thus, the only solution is to synchronize the two USRPs so that the daughter boards can tune to the same reference clock. However, the major problem of the synchronized system is the radar can only be used in a monostatic scenario as there needs to be a synchronizing wire between the two boards.

In communication systems, the phase noise is sometimes estimated from statistical characteristics of the transmitted data sequences. That means a known sequence is sent and based on the statistics of the received sequence, an attempt to estimate the characteristics and model of the phase noise can be made. In radar systems, such estimation is not possible as the transmitter phase noise and the channel phase noise (due to motion) are mixed.

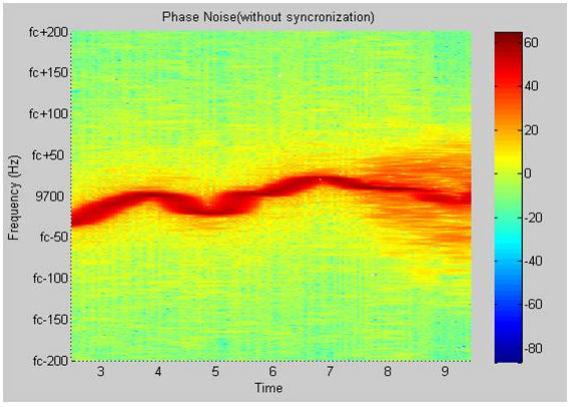

Figure 6.2: Frequency offset and Phase noise in the received signal

The phase noise that results in the received signal at a frequency, f can be given by;

$$L_{phase}(f) = L_{tx}(f) + L_{rx}(f) - 2\rho\sqrt{L_{tx}(f) \cdot L_{rx}(f)}$$

where $L_{tx}(f)$ is the phase noise spectrum of the transmitter , $L_{rx}(f)$ is the phase noise spectrum of the receiver and ρ is the correlation between these phase noise spectra. This derivation is shown in detail for a Doppler radar in [22]. Thus, synchronizing two identical USRPs to obtain $\rho = 1$ completely eliminates the phase noise.

6.3.3 Maximum Distance

The maximum distance of a target that can be monitored using the synchronized experimental platform using two USRPs depends on two factors: the reflected signal to thermal noise ratio (SNR) and the reflected signal to direct signal ratio. The latter ratio can be improved by directional antenna; moreover, it occurs at a localized frequency since the Tx and Rx are synchronized. Thus, let's consider the distance limitation due to the SNR.

The SNR from the reflected echo as a function of distance of the target, R as shown in (3.10). For a synchronized radar in a pseudo-monostatic scenario, (3.10) reduces to:

$$SNR = \frac{P_t \cdot G^2 \cdot \lambda^2 \cdot \sigma}{(4\pi)^3 \cdot (R)^4 \cdot (K \cdot B \cdot T \cdot F)}$$

For our experimental platform, these parameters are as follows: transmitter power, $Pt = 100mW = 20dBm$ maximum, dipole antennas of gain, $G = 1.5(1.76dBi)$, operating frequency of $5GHz$. Analysis done in [27] also shows that the noise figure for the USRP is $F = 2.82$. A receiver bandwidth of $32MHz$ is used since ADC rate is $64MS/sec$.

Using these parameters, the received SNR is given by: $SNR|_{dB} = 60.5 - 40 \cdot \log(R)$. Then, it depends on how much SNR is afforded. For instance, the SNR will be less than 0, only after a distance of $30m$. Hence, the operation range of the platform can be considered roughly to be this distance; even though, there are many factors that can significantly change this range limit.

6.3.4 Maximum Bandwidth

The maximum bandwidth of a signal that the USRP can handle is limited by the sampling rate of the ADC ($64Ms/sec$) . This means based on the Nyquist criterion (to avoid aliasing), the maximum signal bandwidth that can be sampled with this ADC is $64MHz$ if I-Q sampling is used and $32MHz$ if real sampling is used. Hence, a signal of this bandwidth can be sampled and processed in the FPGA.

However, if signal processing is to be done in a processor outside the USRP (in the host PC); the signal must pass through the USB interface, which acts as a bottleneck. USB 2.0 has an effective throughput of 32MB/sec[3]. Since GNU Radio represents each complex sample using 4 bytes (16-bits I and 16-bits Q), this will limit the USB throughput

[3]The maximum data rate of USB 2.0 may reach till 60MB/s , however the effective rate in operation is maximum 32MB/s

to $8MS/sec$. Hence, the maximum bandwidth of a signal that can be sent through the USB is $8MHz$. This is the reason why there are decimation stages in the default FPGA configuration of the USRP.

6.4 Radar Types and Parameters

6.4.1 The Experimental Platform for Different Radar Types

Based on the characteristics of the platform described so far, let's discuss whether the USRP can be used to realize the different radar types of Section 3.4.

***Pulse radar*:** Pulse mode operation with transmission and reception separated in time is not applicable for such a short range application, as the USRP cannot generate very short pulses due to its bandwidth limitation. It is possible to realize a pulse radar using a USRP with both the Tx and Rx operating simultaneously. However, the maximum spatial resolution will be limited to, $\Delta r = \frac{C}{2B} = 18.75m$, which is a very poor resolution for an indoor application. In addition, pulse transmission will result in low average SNR as discussed previously. Hence, pulse radar implementation is not feasible.

***PRS Radar*:** PRS radar will have the same poor resolution as the pulse radar; however, pseudo random sequence transmission will result in a better SNR than pulse radar. This radar is implemented in our platform and some results are obtained for comparison to the CW radar. The only advantage of a PRS radar implemented using the USRP as compared to CW radar is that outdoor interference movements outside the $18.75m$ range can be eliminated.

***CW Radar*:** In CW radar, unmodulated carrier is transmitted; thus, the $8MHz$ bandwidth of the USRP is more than sufficient. Moreover, it has simple implementation and does not have the problems associated with a pulse transmission. Therefore, CW radar is the radar type selected to characterize human movement using the low cost experimental platform.

One of the ways to implement a wideband radar can be to generate and transmit a chirp in the daughter boards; so that the $1GHz$ bandwidth of the daughter boards is utilized despite the low sampling rate of the ADC. However, this approach is not used due to the fact that the oscillators in the daughter boards are not flexible to generate any waveform.

6.4.2 Choice of Parameters

The choice made on some of the parameters in the designed experimental platform is discussed below:

Carrier Frequency: Generally, a higher carrier frequency increases the Doppler frequency resolution, $\Delta fd = 2 \cdot \frac{\Delta Vr}{\lambda}$. On the other hand, lower frequency is preferred to decrease attenuation or to increase the operating distance. In the GNU Radio

based radar, already discussed the choice of carrier frequency is in addition limited by the operation range of the daughter boards, which is in the ISM frequency range $2.4-2.5GHz$ and $4.9-5.9GHz$ for XCVR2450 daughterboard. Therefore, a carrier frequency of $5GHz$ is chosen considering these issues.

Transmit Power: Higher $EIRP$[4] increases the operation range of the radar. However, the $EIRP$ should comply with the power regulation to avoid interference with other systems. More importantly, the maximum $EIRP$ should consider the compliance with the regulations for human exposure to radio frequency. The FCC has set the maximum safety limit of power density to which human beings can be exposed in uncontrolled and controlled/laboratory environment [28]. Since this radar is for an indoor living room environment; the maximum power density allowed is $1mW/cm^2$. If the person goes closer to the antenna than $0.5m$, then it means the $EIRP$ should be limited to, $EIRP < 39dBmW$.

Decimation Factor: As discussed in Section 3.3, a maximum frequency of $200Hz$ is expected from human movement. Hence, a sampling frequency of $Fs = 500Hz$ will suffice. The decimation factor of the decimation stage in the FPGA can be set to a maximum of 256. However, a decimation factor of 128 is used in the FPGA and the resulting signal is again decimated by factor of 1000 in the processor before further analysis.

6.5 Advantages of GNU Radio based Radar

6.5.1 Low Cost

One of the major advantages of the GNU based Radar is that it is low cost. First, the USRP and daughterboard combination is beyond the requirement for a CW radar. Only one of the Tx and one of the Rx channels of the USRP is used. A $64MS/sec$ ADC is more than required for a maximum Doppler frequency of $500KHz$. Thus, a simpler USRP can be designed for a CW radar. In addition, the USRP basically consist of an FPGA which is a low cost component and the daughter boards are based on WLAN chipset technologies which are of low cost because they are produced in large volumes. Thus, if this human activity classifier radar is to be brought to the market ; algorithms will be deployed in the FPGA. The additional components required will be low speed ADC and DAC, WLAN chipsets and antennas. Thus, the hardware components of the radar are generally cheaper.

Secondly, the GNU Radio software is open source and free. Thus, the characterization algorithms can be integrated in real time with the transceiver algorithms in the FPGA. In general a cheap hardware and free software contribute to a low-cost radar.

[4]EIRP is the power radiated off the antenna; thus, this is the power including the gain of the antenna used.

6.5.2 Flexibility

GNU Based Radar is flexible both on the transmission and reception sides provided the flexibilities are satisfied by the RF front-end. Transmission parameters such as transmit power, frequency, waveform type, gain, etc can be controlled. The reception algorithms can also be modified easily. For instance, a new signal processing block can be inserted between already existing blocks as long as the new block is compatible to the signal flow graph. The flexibility of GNU Radio reduces the maintenance and modification cost of the radar. For instance, to convert a GNU Radio based CW radar into a pulse radar, one needs to change only the baseband waveform in the signal generator block from a constant amplitude to a pulse.

Chapter 7

Evaluation & Discussion

It is evident that pseudo random sequence or pulse radars are more suitable to characterize multi-movers and to avoid outdoor interference. However, only CW radars can be implemented in our experimental platform due to the bandwidth limitations discussed in Section 6.3.

Thus, CW radar is implemented in the experimental platform. The human movement characterization methods discussed so far are implemented in MAT LAB and these algorithms are evaluated by making selected experiments in an indoor environment.

In this Chapter, the results from most of the human movement characterization algorithms are presented in the form of plots and discussed. The displacement estimations to quantify movement are evaluated using suitable experiments. Then, the performance of the methods to estimate torso velocity and cadence frequency is tested using the corresponding experiment for movement identification. Finally, the methods to classify activity are evaluated for two human activities: walking and jogging. Thus, it is shown that the parameters obtained from these two different activities are distinct.

7.1 Experimental Setup

The experimental platform consists of GNU radio software that runs on a processor. This software controls the transmitter and receiver parameters including operating frequency, gain and transmit power. We transmit using one USRP setup at $5GHz$ and receive the signal reflected from the moving human being using the other USRP at the same carrier frequency. As discussed in Section 6.3.2, the transmitter and the receiver daughter boards should be synchronized[1] to a common clock. This setup is Figure 7.1.

[1]The synchronization is done by disabling the clock of the slave USRP (by making a circuit modification) and then the clock of the master USRP is fed to the slave using an SMA (SubMiniature version A) connector.

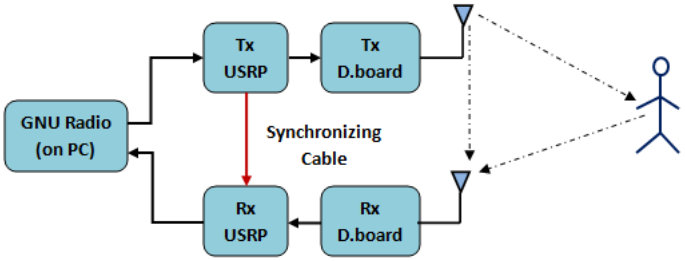

Figure 7.1: Experimental Setup

7.2 Human Activity Quantification

7.2.1 Activity Index

Experiment-1: This is an experiment done in a bistatic scenario. For activity quantification, no synchronization is required; so we placed the Tx and Rx in opposite corners of a room to cover the highest possible area in the room and the test person makes the motion as follows. First, the person keeps static for 6*sec*; then, starts moving randomly between the transmitter and receiver for a time duration of 10*sec* and then stops.

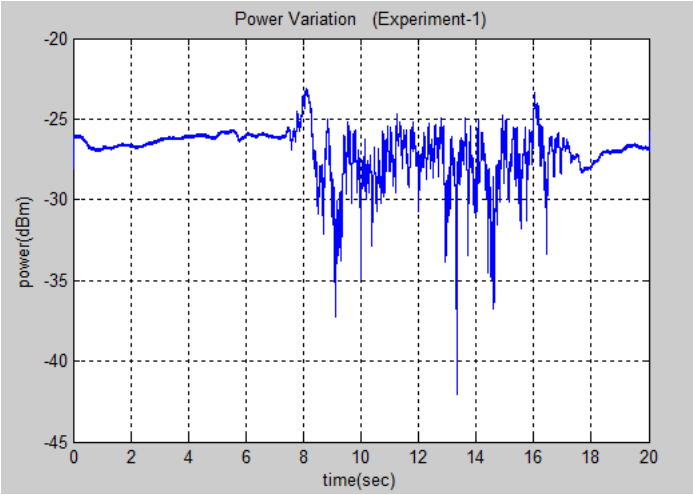

Figure 7.2: Power Variation

The power of the signal obtained and the corresponding activity index estimation is shown in Figures 7.2 and 7.3. The AI estimation shows that the normalized standard deviation is a good estimator of the variation of power and the variation of power can describe the level of activity.

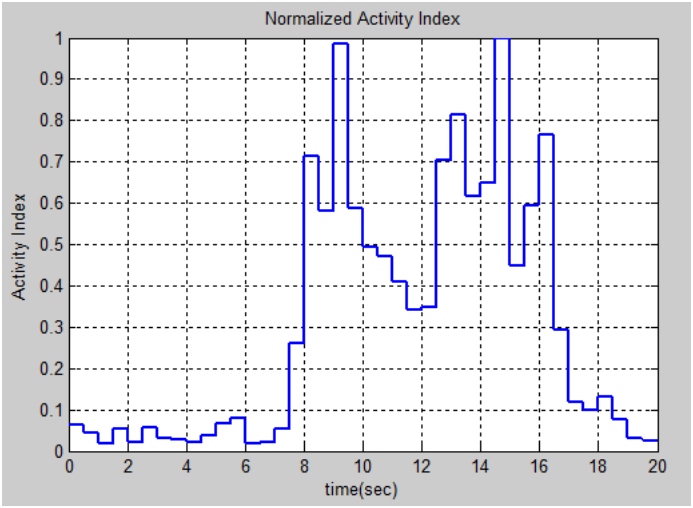

Figure 7.3: Activity Index

7.2.2 Displacement versus Time

Experiment-2: This experiment is done for the scenario shown in Figure 7.4. The person keeps static for $10sec$, and then started moving towards the radar from a distance of about $3m$ in front of the radar. The person follows the motion sequence shown by the dotted arrow for a total time duration of $10sec$. Then, he keeps static at the final point for another $10sec$.

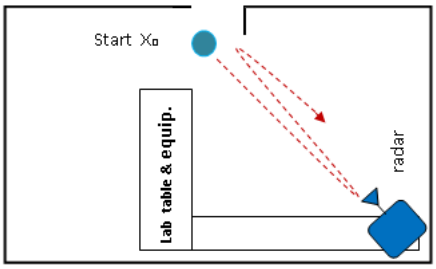

Figure 7.4: Experiment-2

The displacement estimated using the quadrature demodulation method is shown (by the blue line) in Figure 7.5. The figure shows that the displacement estimation follows the motion sequence shown in Figure 7.4. In addition, this displacement estimation is compared in the same figure with a more accurate displacement estimation using the torso velocity estimate as discussed in Section 5.1.2. The figure shows that, the displacement estimate from the simple quadrature demodulation method is as accurate as the one estimated using the torso velocity estimate.

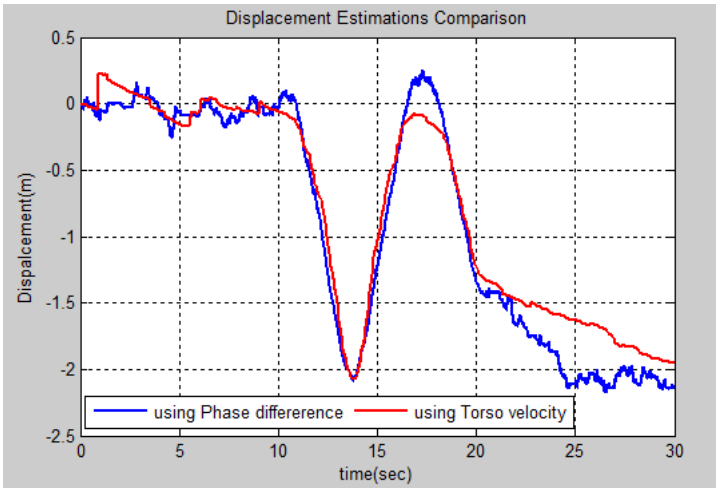

Figure 7.5: Displacement versus time

Experiment-3: The quadrature demodulation method is also verified by a sawtooth motion (a motion that includes tangential motion) in the experimental scenario shown in Figure 7.6. In this experiment, the person keeps static for about $5sec$, and then follows the motion described by the dotted arrow in the corridor. The length of the corridor in which the person moves is $12m$ as the figure shows.

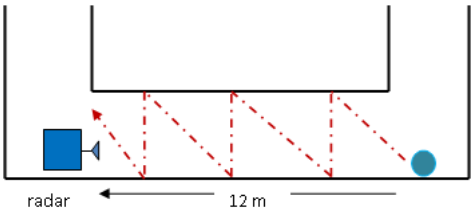

Figure 7.6: Experiment-3

The displacement estimation from this experiment is shown in Figure 7.7. The figure shows that,

- The total displacement till the person reaches the radar (until $22sec$) is about $12.4m$ which gives an estimation error of 3.33% only as compared to the actual distance of $12m$.
- The displacement of the tangential motions remains constant; this shows that the displacement estimator is performing well, as the estimation is for radial displacement.
- The displacement at static condition is overestimated due to coloured noise (clutter) in the first estimation. However, this is completely corrected by using background

subtraction in the second estimation. In the motion range, the two estimations are identical because the background subtraction changes the magnitude of the signal only.

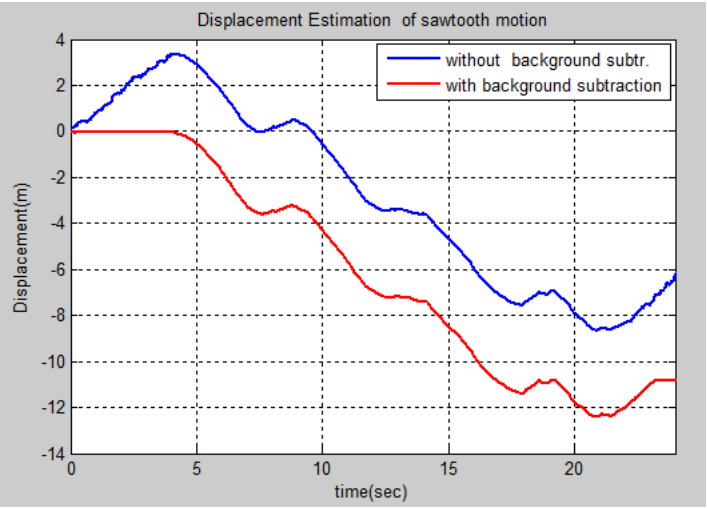

Figure 7.7: Displacement from sawtooth motion

7.2.3 Direction of motion

The spectrogram in Figure 7.8 shows the direction of motion of the person described in Experiment-2 in Figure **7.4.**

A visual inspection of the spectrogram by itself gives much information. The figure shows that the person starts his motion at $10sec$ and moves towards the radar for a time duration of about $3sec$, then turns his direction and moves away for a the radar for a duration of about $3sec$, then pauses for about a sec before moving again towards the radar and finally stops his motion after $20sec$.

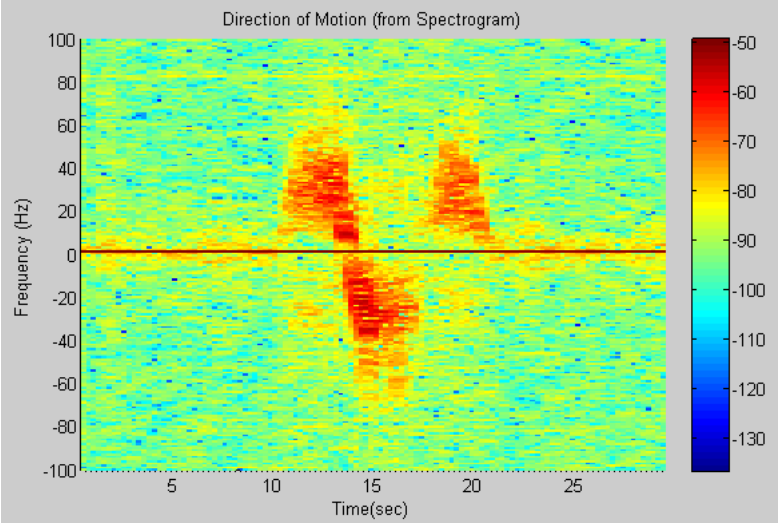

Figure 7.8: Direction of motion

7.3 Human Movement Identification

Experiment-4: In this experiment, the person keeps standing at a distance of $12m$ in front of the radar for some seconds. Then, he starts moving towards the radar at uniform rate. The person starts his motion just before the $12m$ mark and ends few meters after the radar. This experiment is done in a $2m$ wide and $12m$ long corridor as shown in Figure 7.9.

- A timer shows that it takes the person about $10sec$ to complete the $12m$ by walking.
- It is also counted that the person makes 15 steps during this $12m$ walking. Thus, the person moves with $\frac{12}{15} = 0.8m/step$.

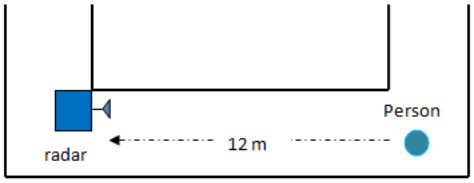

Figure 7.9: Experiment-4

7.3.1 Received Signal

Figure 7.10 shows the real part of the time domain signal recorded during this experiment. The figure shows that the signal level received during static condition (at the beginning)

is very small as compared to the signal level during motion (the next $10sec$). This is due to;

- The directional antenna used that minimizes the direct signal from Tx to Rx.
- The experiment is done in a corridor where possible reflectors (clutter sources) are at farther distance.

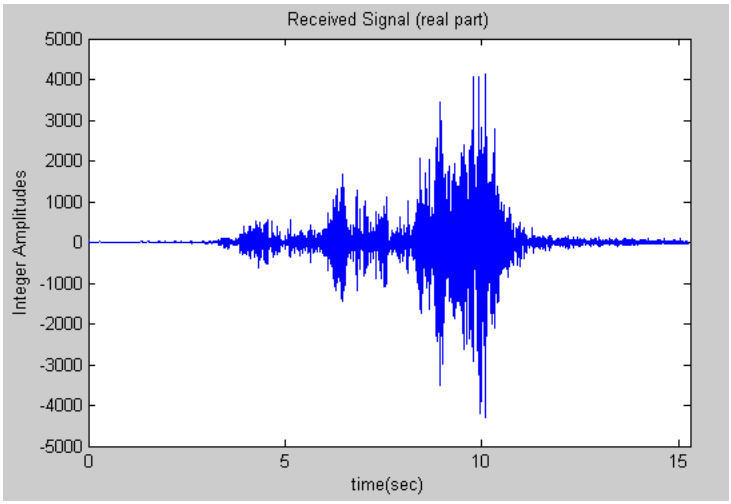

Figure 7.10: Time domain signal

7.3.2 Spectrograms

STFT:

From the spectrogram, two of the parameters recorded manually during the experiment can be clearly observed: the time duration of the motion and the number of steps the person makes. The latter, which is counted to be 15 during the experiment, is equal to the number of spikes in the spectrogram.

In addition, the multipath effect shown in Figure 3.2 is evident from this spectrogram as the negative Doppler frequencies are filled with the image Doppler pattern, but with lower power levels.

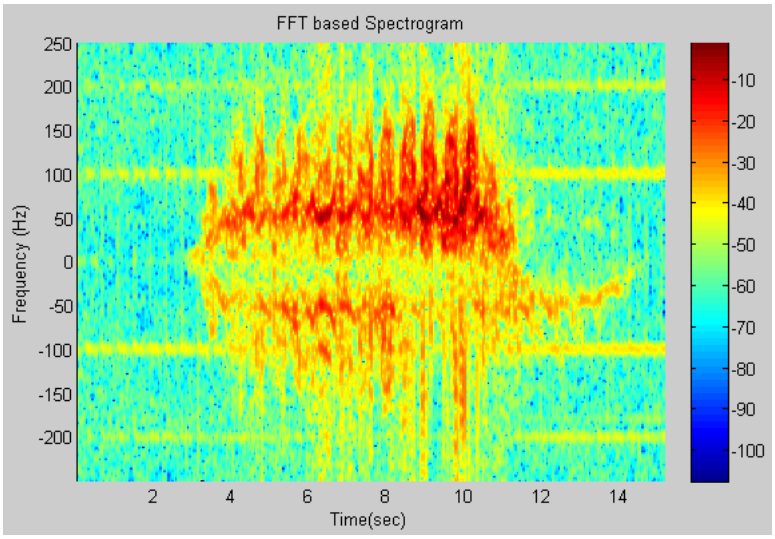

Figure 7.11: STFT based Spectrogram Estimation

Sliding Window MUSIC:

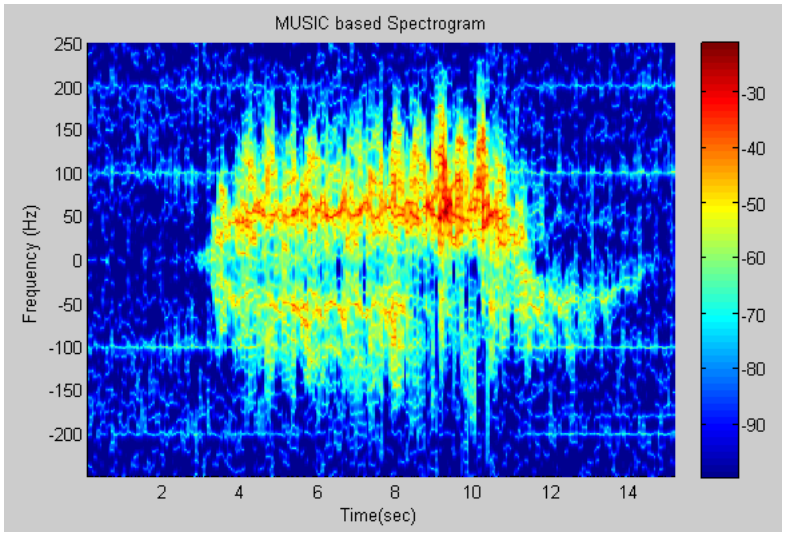

Figure 7.12: MUSIC based Spectrogram estimation

It is clearly visible from the MUSIC based spectrogram that:

- The spectrum is resolved in frequency domain; i.e., the stronger frequencies are clearly visible within the pattern.
- In the time domain, continuity of reflections from body parts is seen.

The following estimations are based on the MUSIC based spectrogram shown above as it has better frequency resolution than the STFT based spectrogram. The MUSIC spectrogram during motion, i.e., between 3 and 11sec is taken to verify torso velocity estimation and to estimate the cadence frequency of the gait.

7.3.3 Torso Velocity

The velocity estimations of the motion described in Experiment-4 are shown in Figure 7.13.

- To verify this velocity estimation, let's take a part of the motion where the torso velocity, $v_{torso}[n'] > 0$, i.e., the time range the person was moving towards the radar. Thus, the distance the person moves can be estimated as the area under this velocity versus time graph. That is, $Distance = \Delta n' \cdot \sum_{n'=3sec}^{8sec} v_{torso}[n']$. This gives,
  - $Distance = 13.26m$, using estimation based on maximum power, which gives an error percentage of only10.5% as compared to the actual distance of $12m$.
  - $Distance = 11.34m$, using estimation based on weighted average, which gives an error percentage of only 5.5%.
- These results show that both torso velocity estimation methods give good results. From the figure (the estimation using maximum power), we see an up and down velocity trajectory of the torso during the walking. This is true as the torso moves a little forward (increase in velocity) and a little backward (decrease in velocity) even when the whole body is moving at constant velocity.
- The torso velocity, $v_{torso}[n']$ is almost equal to the body velocity, $V[n']$. Thus, the average velocity of the body can be estimated by taking the average value of the torso velocity over the motion interval, which is between $3sec$ and $11sec$ as shown in the Figure 7.13. i.e.,

$$V_{body} = average(v_{Torso}) = 1.422m/sec$$

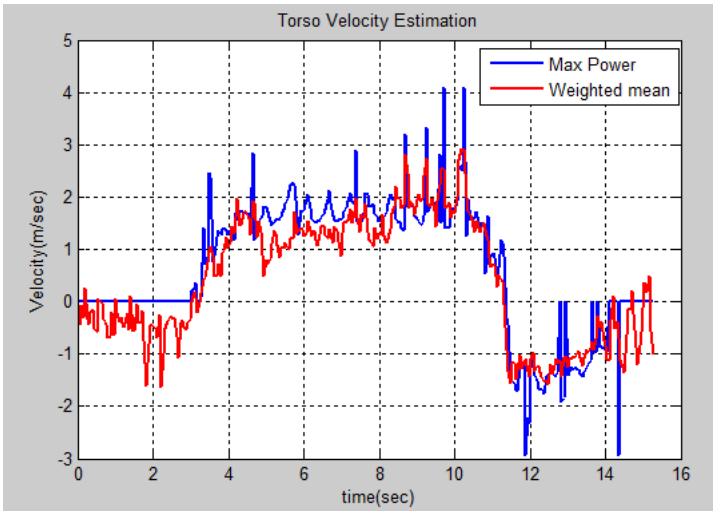

Figure 7.13: Torso velocity Estimations

7.3.4 Cadence Frequency

The cadence frequency spectrogram obtained from the time domain spectrogram is shown in Figure 7.14.

The cadence frequency shows the rate at which the power at each Doppler frequency changes through time. For instance, we see that the Doppler frequency around $50Hz$ $(1.5m/sec)$ is the strongest and it exists at the 1^{st} bin of cadence frequency (at $f_c = 0$). All the body parts contribute to this zero cadence as each body part is moving according to the velocity profile shown in (2.1).

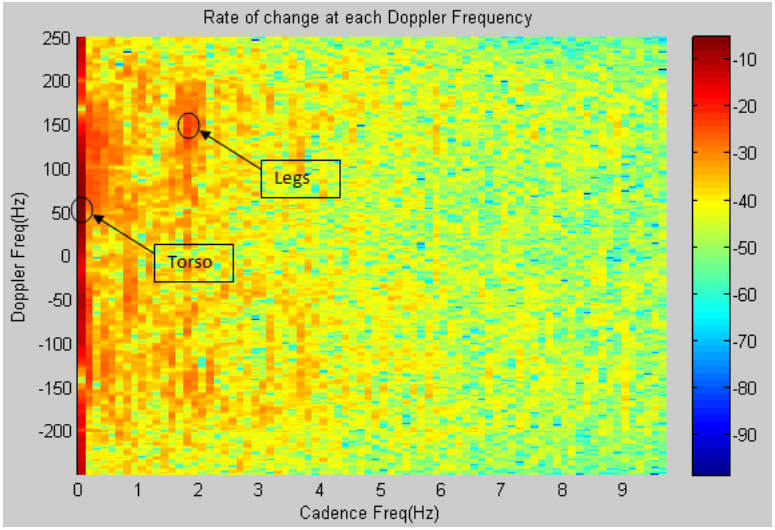

Figure 7.14: Doppler vs cadence frequency

Cadence of the gait:

The cadence of the gait is obtained by summing the powers from $f_k = 0$ to $f_k = 250Hz$ at each cadence frequency. This gives the cadence frequency plot shown in Figure 7.15.

As expected the cadence frequency has the highest power at $f_c = 0$. The fundamental cadence of the gait is equal to the second peak in the cadence frequency plot. Thus, the gait cadence: $f_c = 1.74Hz = 1.74steps/sec$ from Figure 7.15.

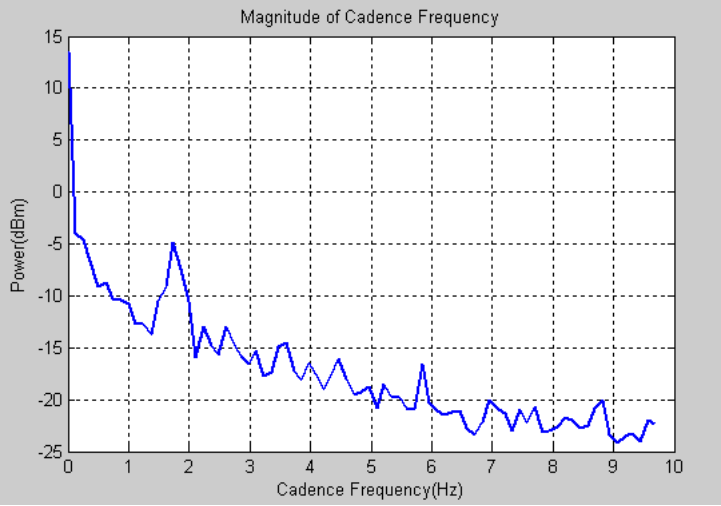

Figure 7.15: Cadence frequency

Step Length:

- The step length is the ratio of the velocity of the body to the cadence frequency. Hence, the step length is equal to $S_l = \frac{V_{body}}{f_c} = \frac{1.422m/sec}{1.74steps/sec} = 0.82m/step$.
- Thus, the estimation error of the step length as compared to the actual step length of $0.8m$ is only 2.44%.

7.4 Human Activity Classification

Experiment-5: The objective of this experiment is to verify that the parameters of human motion will have different values for different human activities. The experiment is done in a large room. In this experiment, a person starts his motion from a distance of about $15m$ and moves towards the radar until he stops few meters behind the radar. Three types of activities are done walking, jogging[2] and making exercise standing at half-way distance. The person covers the same distance while making the walking and jogging experiments.

[2]Jogging means running at a slow or leisurely pace.

7.4.1 Spectrograms

The spectrograms obtained from the three activities are shown in Figure 7.16.

- The spectrogram from the different activities are quite distinct.
- It is also evident from the figure that, the jogging spectrogram has a smaller time range than walking spectrogram (as expected).

To obtain the parameters for activity classification, 4*sec* of data from the interval 2*sec* to 6*sec* of the MUSIC based walking and jogging spectrogram shown in Figure 7.17 are taken.

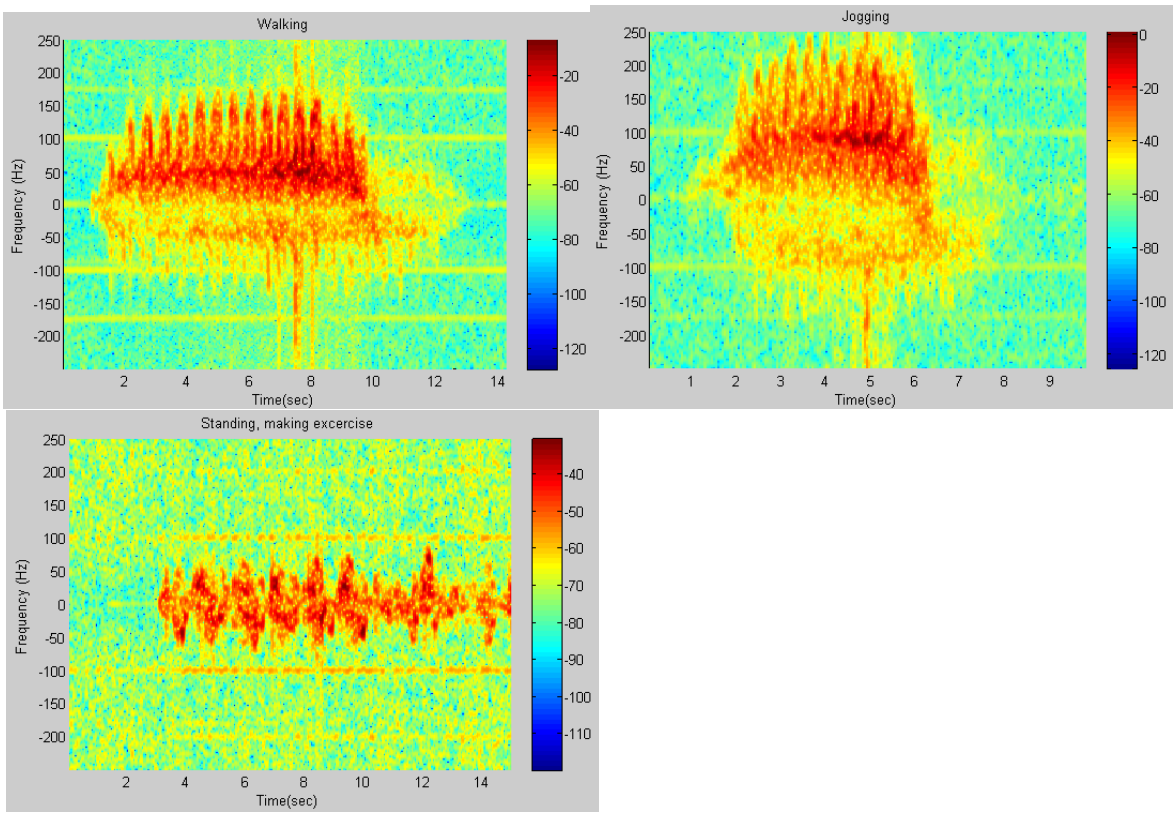

Figure 7.16: Spectrograms from different Activities

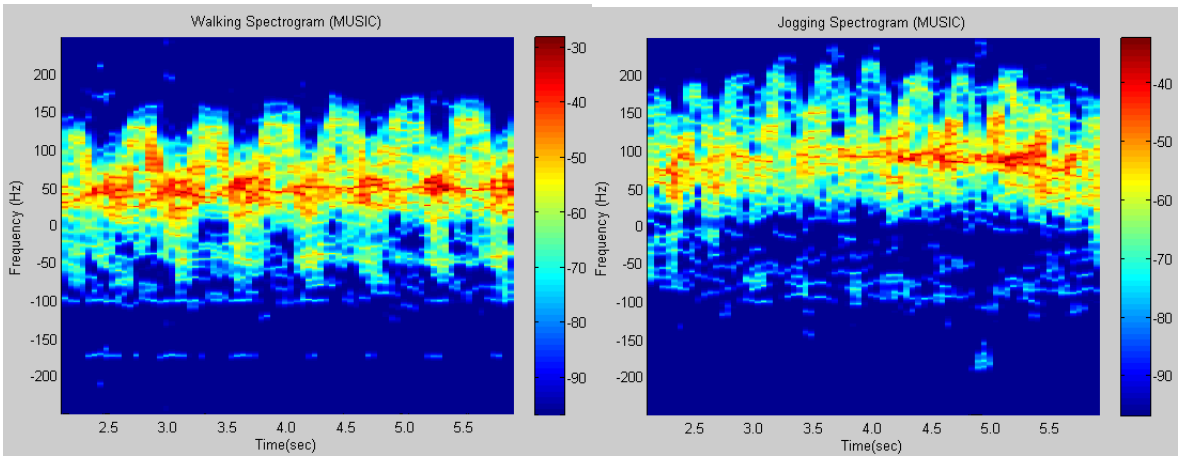

Figure 7.17: MUSIC spectrograms for walking and jogging

7.4.2 Torso Velocity

The torso velocity estimations are shown in Figure 7.18. Thus, averaging over the $4sec$ time interval gives, a body velocity of;

- $1.61m/sec$ for the walking experiment.
- $2.56m/sec$ for the jogging experiment.

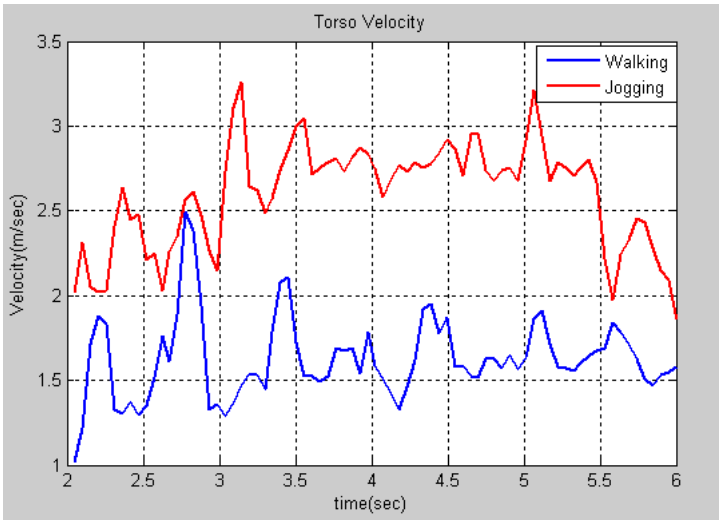

Figure 7.18: Classification based on torso velocity

7.4.3 Step Length

The cadence frequency estimation from the two activities is shown in Figure 7.19. By picking the 2^{nd} significant peak in the cadence frequency plot, the cadence frequency is found to be $1.73 steps/sec$ for walking and $2.47 steps/sec$ for jogging. Hence, the step length is;

- $S_l = \frac{v_{torso}}{f_c} = \frac{1.61 m/sec}{1.73 steps/sec} = 0.93m$ for the walking experiment.
- $S_l = \frac{v_{torso}}{f_c} = \frac{2.56 m/sec}{2.45 steps/sec} = 1.05m$ for the jogging experiment.

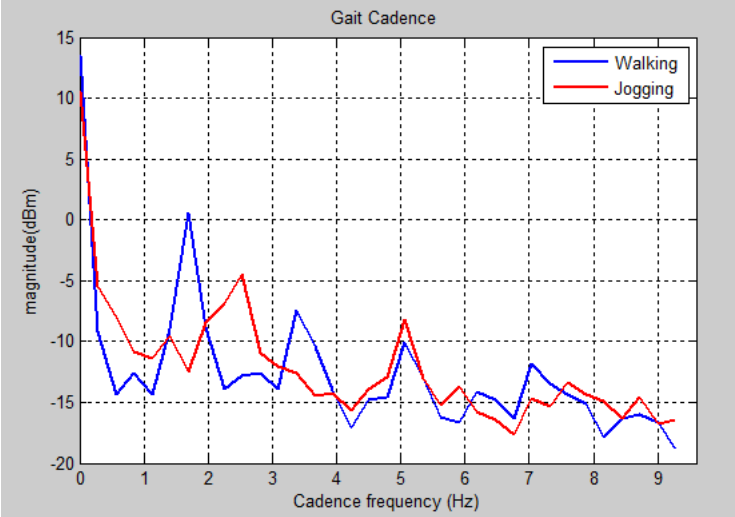

Figure 7.19: Cadence frequency of the gait

7.4.4 Velocity Bandwidth

The velocity envelopes of the two activities are shown in Figure 7.20. Since the negative frequencies are due to multipath, the velocity envelopes are extracted from the positive Doppler frequency part of the spectrogram only.

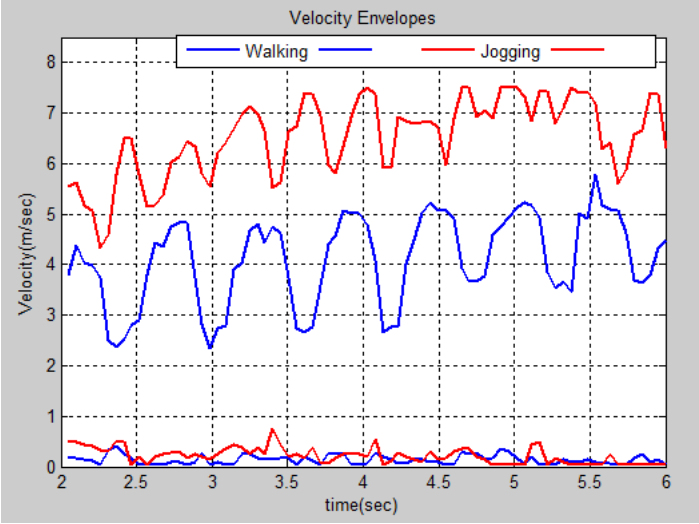

Figure 7.20: Classification based on velocity envelopes

From the upper and lower envelope estimations, $f_{UE}[n']$ and $f_{LE}[n']$, the velocity bandwidth with and without micro-Doppler can be estimated.

- Micro-Doppler velocity bandwidth = $average\{maxima(f_{UE}) - minima(f_{LE})\}$, which gives:
  - 4.53 m/sec for walking
  - 6.46 m/sec for jogging
- Velocity bandwidth without micro-Doppler = $average\{minima(f_{UE}) - maxima(f_{LE})\}$, which gives:
  - 2.75 m/sec for walking
  - 5.28 m/sec for jogging
- Offset of the velocity spectrum = $average\{maxima(f_{UE}) + minima(f_{LE})\}$, which gives:
  - 2.47 m/sec for walking
  - 3.56 m/sec for jogging

It is logical that the velocity bandwidth from jogging is greater than that of walking as the body will move with a wide range of frequencies during running than during walking.

The fact that the velocity offset for both activities is greater than the torso velocity shows that there is a higher velocity forward swing than backward swing in the human locomotion.

7.4.5 Standard Deviation

The standard deviation of the power over the velocities with the velocity bandwidth is shown in Figure 7.21 for the two activities involved.

The average standard deviation over the $4sec$ interval is $10dB$ for walking and $14dB$ for jogging. Thus, the variation of power over the velocity components of the motion can also be used as a parameter for classification. This is also related to the appendage to torso ratio, ATR parameter. That means, low ATR will result in higher standard deviation than high ATR.

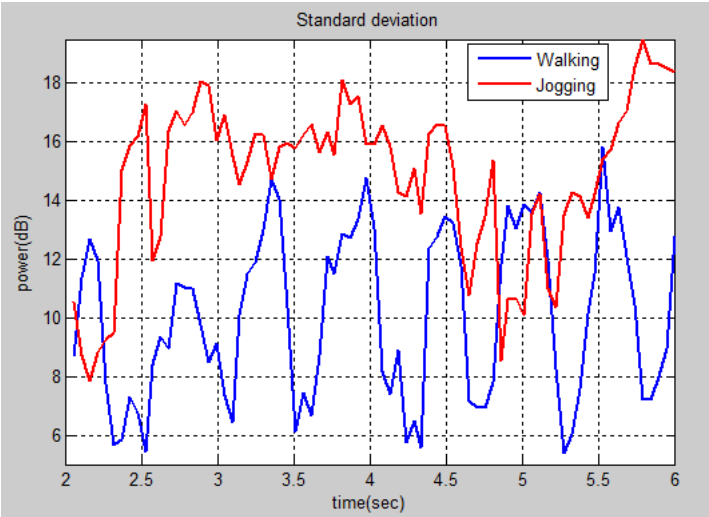

Figure 7.21: Standard deviation of power within velocity bandwidth

7.5 Velocity Profile

In the following methods, an attempt is made to extract the velocity profile points of the walking in Experiment-5 as discussed in Section 5.4. The velocity profile points of the motion obtained from the local maxima of the MUSIC based spectrogram are shown in Figure 7.22 for a threshold[3] of $5dB$.

Combination of these local maxima through time should lead to a velocity profile that is close to the model based profile in Figure 2.1. Then, the points are arranged in order of their powers and tracking with time is done to obtain the set of points which describe the velocity profile of each body part, $v_m(t)$ as discussed in Section 5.4. However the strongest power based tracking did not give smooth velocity profiles. Thus, another method to construct the velocity profile points from the maxima obtained should be sought for.

[3] a value is taken as a maxima if it exceeds its neighbor values by more than the threshold.

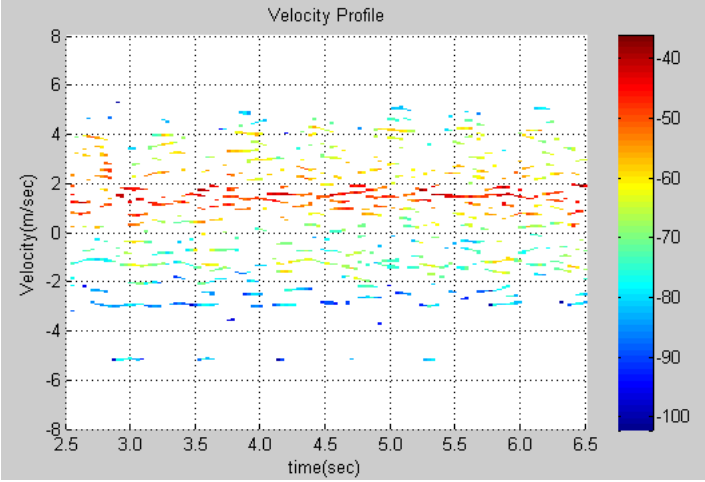

Figure 7.22: Velocity Profile using local maxima in MUSIC

7.6 Conclusion

From the results of the experiments performed, the following points can be concluded:

- It suffices to monitor the normalized standard deviation of power to get information about the level of activity in an indoor environment.
- The two path model of quadrature demodulation is accurate enough to get a rough estimation of the displacement of a person. This method is quite simple as compared to distance estimation methods which use a short pulse analysis.
- Parametric spectral estimators are more useful and superior as compared to the non-parametric ones for movement parameter extraction. For some of the parameters, these estimators perform the same; however, some of the parameters that require high resolution, such as standard deviation within the velocity bandwidth, benefit from the parametric estimators.
- The methods to obtain velocity and step length of the body give good estimations for radial motion of the person.
- Parameters such as torso velocity, step length, velocity bandwidth are found to be distinct for the different human activities performed; therefore, these parameters can be used in training classifiers for automatic classification.
- The velocity profile of the different body parts can be obtained from the spectrogram; however, better tracking methods to match the velocities in consecutive windows are required.

Chapter 8

Conclusions & Future Work

8.1 Conclusion

In this thesis, parameters of human motion that can be used for activity quantification, identification and classification are summarized using human movement models. The Doppler shift phenomenon is utilized to measure human movement pattern using radar. The Doppler signal model due to human motion in a multipath environment is derived in a general bistatic radar scenario. It is found that the human motion, especially in an indoor environment, consists of a wider Doppler spectrum than the motion of rigid objects. The Doppler model is then utilized to compute a useful representation of the motion: the spectrogram, using non-parametric and parametric estimators. It is found that the sliding window MUSIC spectrogram has better resolution and hence it is more useful in calculating most of the parameters than the STFT based spectrogram. It is also discussed that the background clutter spectrum can be estimated in a static condition and thus, it can be subtracted from the spectrogram.

The results obtained show that quadrature demodulation with background subtraction is a good but simple displacement estimator. The displacement estimate can be a simple solution to find the position of a human target especially if displacement estimates from distributed radars can be combined. It is also shown that human activity can be identified from other kind of movements in an indoor environment by using the torso velocity profile and cadence frequency estimates obtained from the spectrogram. It is also concluded that, the parameters of motion obtained from the spectrogram such as torso velocity, cadence frequency, velocity bandwidth are distinct enough to allow classification of human activities. Thus, a classifier can be trained using these parameters for efficient automatic classification.

It is also concluded that an indoor short range radar can be implemented using simple transceivers like USRP. As already discussed, GNU Radio based radar is low-cost and flexible. Unmodulated continuous wave radars can sufficient to characterize human motion; however, modulated radars with a higher bandwidth are required to discriminate multi-movers.

8.2 Future Work

The following points are recommended as future work:

***Classifier Training*:** Parameter extraction is one major step towards classification or identification. However, it is difficult to find some defined unique range for these parameters for the different activities. Thus, classification can only be done by training the classifier with a series of experimental data taken for each activity; so that most likely hood classification can be done in a real scenario. Thus, this work can be extended by selecting a suitable classifier and making experiments to get statistical data for the classifiers.

***Phase Noise*:** Most of the validation experiments are done using a synchronized transmitter and receiver arranged in a pseudo-monostatic scenario. However, it may be required to operate a radar in a bistatic scenario so that most of the indoor environment is covered. However, there will be phase noise and frequency offset due to oscillator drift which makes extraction of small velocities, like those from the human motion, impossible. The frequency offset can be removed by estimating the offset of windowed segments of the signal using STFT. However, solving the phase noise problem in a bistatic scenario requires further study.

***Distributed Radars*:** Radar measures a radial motion pattern. Most of the identification and classification parameters obtained such as torso velocity, displacement, etc., represent the radial component of these parameters. The activity index computed may not equally represent motion in different parts of the room; moreover, the motion pattern received from a person behind walls can be too noisy. Thus, one of the solutions to reduce these problems is deploying more than one radar (distributed radars). This could involve deploying more than one transmitter or more than one receiver. Thus, the efficient combination of Doppler information from these radars can lead to an estimate more close to the actual values of these parameters.

***Multi-movers*:** Most of the methods suggested in this thesis face a problem in the presence of multiple persons. Different ways could be suggested to solve the problem:

- *Antenna arrays*: One way is to use antenna arrays (at least duplets) even though it could be expensive. Thus, the variability of the spatial response of the antenna arrays through time can be analyzed to see the direction of movement of the movers. Another way using antenna arrays is combining the spectrograms from each antenna; so that the phase difference, and hence the DOA, can be obtained at each Doppler frequency at a particular time. Combining these three parameters yields DOA versus frequency versus time information. From such a plot, the movement of the persons can be discriminated. This SIMO (single input multiple output) system can also be implemented using a USRP as there are two receiver sections in the USRP.

- *UWB Radars*: The use of UWB radars will enable a 3-D, Range-Time-Frequency analysis. That means, the range bin at which the legs, arms, head or torso are present can be singled out and separate time-frequency plots of each body part can be obtained. This will make both identification and classification of human activities accurate. Therefore, the use of UWB radars for human activity identification and classification is highly recommended. However, translation motion of the person will lead to migration of the required bin making the bin tracking challenging. Tracking of the required bin based on power level or selecting a bin common to the selected consecutive oscillations can be a possible approach. However, UWB radars could be too expensive; moreover, wideband radars are sufficient for discriminating multi-movers.

- *High sampling rate ADC*: The cheapest way for multi-mover detection is using a higher rate ADC than the current $64MS/sec$ ADC in the USRP. It can be said that, we don't need a resolution more than $0.5m$ to discriminate multi-movers. Thus, such a resolution can be achieved by $300MS/sec$ ADC for instance. However, a fast ADC means all the signal processing should be done in the FPGA.

Therefore, our recommendation for multi-mover detection is to use a high sampling rate ADC together with the USRP as a pseudo-random sequence radar (this radar is already implemented in GNU Radio as part of this work, but not used in the results because the spatial resolution is not useful enough because of the low sampling rate ADC).

Bibliography

[1] K.Lukin, V.Konovalov, "Through the wall detection and recognition of human beings using noise radar sensors", *Institute of radio physics and electronics*, Oct. 2004.

[2] P. Lay, M.Narayanan, "Through-wall imaging and characterization of human activity using ultra wideband random noise radar", *Proc. of SPIE*, 2005.

[3] Micheal G. Anderson, "Design of multiple frequency continuous wave radar hardware and micro-Doppler based detection and classification algorithms", *PHD dissertation, University of Texas at Austin*, May 2008.

[4] Otero,M.,"Application of a CW radar for human gait recognition", *Proc. of SPIE,* vol.5788, 2005.

[5] Z.Gurbuz, L.Melvin, B.Williams, "Detection and identification of human targets in radar data", *Proceedings of the SPIE,* vol. 6567, 2007.

[6] C. Hornsteiner, J.Detlefsen, "Extraction of features related to human gait using a continuous wave radar", *German Microwave Conference*, 2008.

[7] C. Hornsteiner, J.Detlefsen, "Characterization of human gait using a continuous wave radar at 24GHz", *Advances in Radio Science*, vol. 6, pp.67-70, 2008.

[8] Y.Kim, H.Ling, "Human activity classification based on micro-Doppler signatures using an artificial neural network", *IEEE Antennas and Propagation Society International Symposium*, July 2008.

[9] J.Geisheimer, W. Marshal, E. Greneker, "A CW radar for gait analysis", *IEEE Signals, Systems and Computers conference*, vol. 1, pp. 834-838, 2001.

[10] Lay, Ruan, Narayanan, "Hilbert-Haung Transform processing of through wall noise radar data for human activity characterization", *International symposium on Signals, Systems and Electronics*, pp. 115-118, July 2007.

[11] L.Du, P.Stoica, H.Ling, S.Ram, "Doppler spectrogram analysis of human gait via iterative adaptive approach", *Electronics Letters*, Vol. 45, Issue 3, pp. 186-188, Jan. 2009.

[12] Adrian Lin, "Low complexity radar for human tracking", *PHD Dissertation, University of Texas at Austin*, May 2006.

[13] A.Lin, H. Ling, "Doppler and direction of arrival radar for multimover sensing", *IEEE Transactions on Aerospace and Electronic Systems*, vol. 43, Issue 4, pp. 1496-1509, Oct. 2007.

[14] S.Ram, Y.Li, A.Lin, H. Ling, "Doppler-based detection and tracking of humans in indoor environment", *Journal of the Franklin Institute* 345, pp. 679-699, 2008.

[15] R.Boulic, N.Thalmann, D. Thalmann, "A global human walking model with real-time kinematic personification", *The Visual Computer Journal*, vol. 6, 1990.

[16] Z. Zonghua, N. Troje, "3D periodic human motion reconstruction from 2D motion sequences", *Proceedings of IEEE computer society workshop*, 2004.

[17] M.I. Skolnik, Introduction to radar systems, 3rd edition, McGrawHill Book Co.

[18] Eugene F. Knott, John F. Shaeffer, Michael T. Tuley, "Radar Cross Section", Second Edition.

[19] J.Geisheimer, W. Marshal, E. Greneker, "High-resolution doppler model of the human gait", *Proc. SPIE*, vol. 4744, 2002.

[20] M. Murray, A. Drought, R.Korry, "Walking patterns for normal men", Journal of bone and joint surgery.

[21] E. Andrade, "Doppler and Doppler effect", *ICI London*, vol. 18, No. 69, Jan. 1959.

[22] T.Wu, H.Tang, F.Xiao, "Research on coherent phase noise of millimeter-wave Doppler radar", *Progress in Electromagnetic research letters*, vol. 5, pp. 23-34, 2008.

[23] R.Crochiere, L.Rabiner, "Optimum FIR Digital Filter Implementations for Decimation, Interpolation, and Narrow-band filtering", *IEEE transactions on Acoustics, Speech, and Signal Processing*, vol. 23, Issue 5, pp. 444-456, Oct. 1975.

[24] P.Stoica, R.Moses, Introduction to Spectral Analysis, Prentice Hall edition,1997.

[25] S.Mcolash, J. Heinen, R. Niederjohn, "A spectral subtraction method for the enhancement of speech corrupted by non-white, non-stationary noise", *IEEE Proc. on industrial electronics, control and instrumentation*, vol. 2, pp. 872-877, Nov. 1995.

[26] M. Berouti, R. Schwartz, J. Makhoul, "Enhancement of Speech Corrupted by Acoustic Noise", *IEEE International Conference on Acoustics, Speech, and Signal Processing*, Apr. 1979.

[27] Lee K. Patton, "A GNU radio based Software Defined Radar", *MSc Thesis, Wright State University,* 2007.

[28] "Questions and answers about biological effects and potential hazards of Radio frequency Electromagnetic fields", *FCC OET bulletin* 56, Aug. 1999.

[29] Firas A. Hamza, "USRP under 1.5x magnifying lens", GNU Radio community.

[30] Matt Ettus, "USRP users and developer's guide", Ettus Research LLC.

[31] D. Shen, "How to write GNU Radio python applications", 2005.

Appendix A

Universal Software Radio Peripheral

> **Note:** The hardware description of the USRP and daughter boards is mostly based on the information I read and learned from GNU Radio forums and based on the guides: [27], [29] and [30]. I would like to thank these authors for their volunteer contribution as their is no a standard manual for the USRP and daughter boards.

USRP is a general purpose radio that allows general purpose computers to function as software defined radios. It can be directly plugged through USB to the host processor. USRP[1] is designed such that it serves as a digital baseband and IF section of a radio communication system . The USRP consists of a cyclone FPGA, which makes it general purpose, flexible and easily controllable. There are different daughter boards that are designed to function as an RF section of the USRP. Figure A.1 shows how the USRP is used with four daughter boards. The gain and carrier frequency of these daughter boards can also be controlled from the host processor through the USRP.

A.1 The USRP

The USRP is designed such that the high speed signal processing, such as down conversion, up conversion, decimation, interpolation, filtering are done in the FPGA. The low speed signal processing such as modulation, demodulation and further signal processing takes place in the host processor. This avoids bandwidth limitation due to USB bottleneck and lessens computational burden of the processor.

The main components of the USRP are four DACs, four ADCs, Altera Cyclone EP1C12 FPGA and Cypress FX2 USB 2.0 interface chip. The GNU radio community mainly uses the USRP for wirelsess communication research. As a result, they have designed a default FPGA configuration that is suitable for most communication systems. The USRP with this default FPGA configuration is shown in Figure A.2. The figure shows that the USRP has independent transmit and receive paths.

[1] USRP is designed and currently sold by Mr. Matt Ettus, http://www.ettus.com

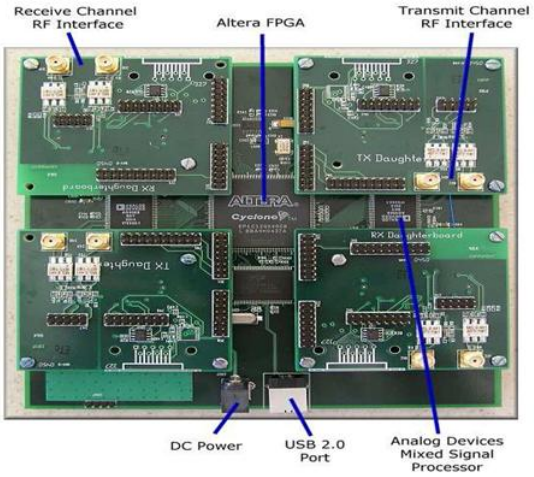

Figure A.1: The USRP with basic transmit and receiver Daughter boards

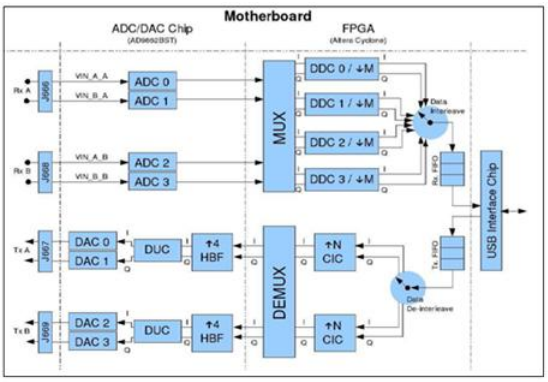

Figure A.2: USRP motherboard

The Receiver daughter boards, the RF front ends for the USRP will be plugged to RxA and RxB and the transmitter daughter boards to TxA and TxB slots. As shown, the in-phase and quadrature components of the signal have separate paths and ADCs. The USRP uses 32-bits to represent a complex sample (16-bit in-phase and 16-bit quadrature); hence, the samples received in the host are signed integer values instead of actual voltage values.

The Transmit Signal Path

The complex data symbols to be transmitted are represented in an integer format and sent to the USB. The USB interface chip stores these data in a FIFO transmit buffer. Then, these data is interleaved and fed to the CIC (Cascaded Integrate-Comb) interpolator. If the user specifies an interpolation factor of N, the CIC interpolators interpolate by a factor N/4 and the remaining factor of 4 is done by the half band filters (HBF). The

De-multiplexer then determines to which digital up converters the data will be output. The digital up converters convert the base band data to an IF frequency. These data is then converted to analog by $14 - bit$, $128MS/sec$ DACs. The DAC can output a maximum power of $10dBm$[2]. There is also a programmable logic controller (PGA) that can amplify the signal by a gain of up till $20dB$ after the DAC. Then, these signal is RF modulated and transmitted by the daughter boards.

The digital up converter section shown in Figure A.3, converts the base band analog signal of frequency,ω_o to a passband RF signal. If a symbol,$S_n = a_n + jb_n$is transmitted then the output, $R_n$will be given by,

$$R_n = a.\cos(\omega_c) - b.\sin(\omega_c) + j\left\{a.\cos(\omega_c) + b.\sin(\omega_c)\right\} = S_n.e^{j\omega_c}$$

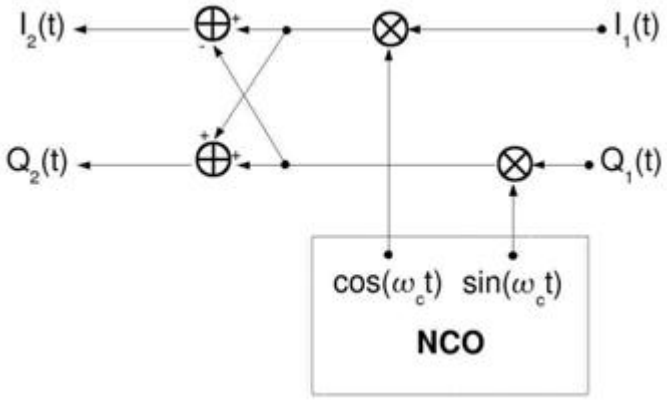

Figure A.3: Digital Up converter in USRP

The Receive Signal Path

In the receive signal path, the analog IF signal is received from a quadrature[3] daughterboard plugged to RxA or RxB. This IF signal is sampled by $64MS/sec$, $12 - bit$ ADC. The full range of the ADC is $2V$ peak to peak across a 50Ωdifferential resistor. This means the maximum power of a signal that can be sampled with the ADC without clipping is $16dBm$; however there is a programmable gain amplifier (PGA) of $20dB$ before the ADC to amplify low level received signals. Then, the value of the multiplexer in the FPGA determines from which ADC the input of each DDC (digital down converter)[4] will be taken. The output of the DDC is interleaved and stored in the Rx, FIFO buffer. Then, the data will be stored or processed in real time in the host PC.

The digital down converter section consists of a frequency down converter and a decimator as shown in Figure A.4. The higher frequency components are first filtered

[2]The DAC supplies maximum of 1V peak-to-peak to a 50Ωresistor
[3]a daughterboard which has both in-phase and quadrature signal components
[4]only DDC0 and DDC1 are currently being used in the default FPGA configuration

out using a four-stage CIC filter and decimated by factor $M/2$, where M is the decimation factor set by the user. The remaining factor of 2 decimation is done by the HBF.

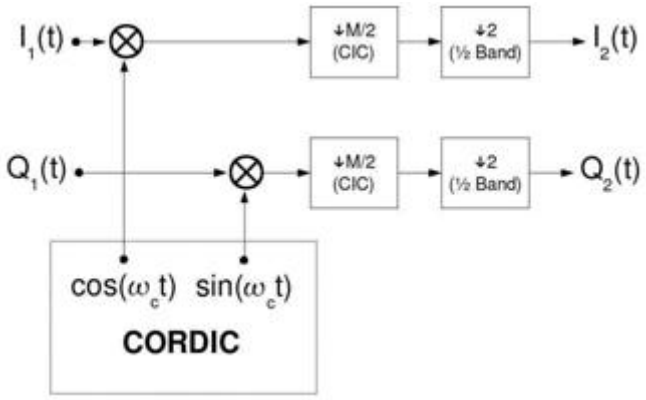

Figure A.4: Digital down converter section in USRP

The USRP has the following features in general:

- Has an FPGA which can be designed into any Rx or Tx component.
- The multiplexer value, the interpolation and decimation rates, the gain and other settings can be set by software.
- It has high speed analog to digital converter which can sample signals of bandwidth till $64MHz$ without aliasing.

A.2 Daughter boards

There are different types of daughter boards that can be used as an RF front-end on the USRP. The main differences between these boards include:

- Maximum transmit power
- Operation frequency range
- The number of transmit and receive sub-devices[5] contained
- Whether the board uses its own or the motherboard (USRP) clock.
- Cost

The following are the major daughter boards designed by Ettus Research and used nowadays together with USRP.

[5]A sub-device is an independent transmitter or receiver part within a daughterboard which can be tuned and whose gain can be set.

Daughterboard	Function	Operating Frequency (MHz)	Transmit power	Clock	Cost
XCVR2450	Transceiver	2400-2500 & 4900-5900	20dBm	USRP	$275
RFX2400	Transceiver	2300-2900	17dBm	self	$275
DBSRX	Rx	800-2400	.	USRP	$150
LFRX/LFTX	Rx/Tx	0-30	.	.	$75
Basic Rx/Basic Tx	Rx/Tx	2-200	.	.	$75

Table A.1: USRP Daughter boards and their Characteristics

Most of the daughter boards are direct down conversion daughter boards, meaning they can translate the RF signal directly to a base band signal. Moreover, some of them use the USRP clock and some of them their own clock as reference. So, the tuning method varies from daughterboard to daughterboard.

We used XCVR2450 daughterboard together with USRP. RF down conversion in this board is discussed as follows.

Tuning in XCVR2450 This daughterboard is a direct down conversion daughterboard. There is a voltage controlled oscillator (VCO) in the board that is controlled by a Phase locked loop (PLL) based frequency multiplier which takes the USRP clock as reference as shown in Figure A.5. When the user sets the receive or transmit frequency of the daughterboard to a frequency,f ; the PLL based frequency synthesizer tries to set the VCO frequency as close as possible to the required frequency using the loop filter. Finally the VCO frequency will be set to a multiple of the USRP oscillator frequency and with a phase equal to the phase of the USRP Oscillator[6]. If the required tuning frequency can be done to the multiplier resolution of the PLL then direct down conversion will occur and the DDC frequency in the FPGA will be set to 0. Otherwise, tuning will be done in the XCVR as close as possible to the the required frequency and the remaining tuning is done by the DDC in the FPGA.

[6]The USRP oscillator is a 64MHZ, 20ppm(parts-per-million) oscillator in the motherboard

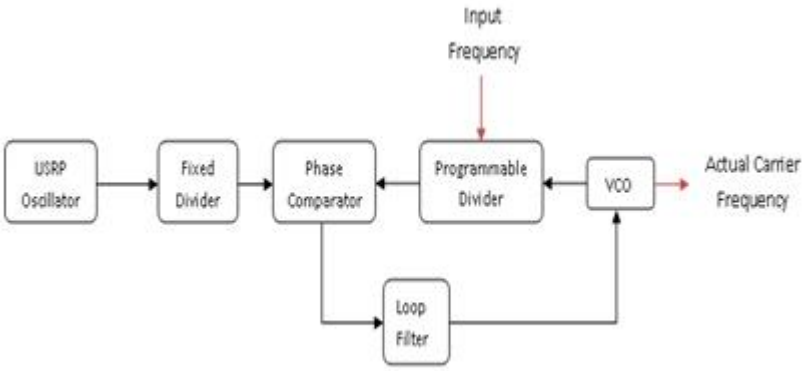

Figure A.5: PLL based frequency multiplier

Appendix B

GNU Radio

B.1 Introduction

GNU Radio is an opensource,free software toolkit to build and deploy software defined radios. The software consists of a set of hardware independent signal processing blocks and hardware dependent interface code that links up the signal processing blocks running on a general purpose computer with the USRP hardware. GNU Radio has signal processing libraries written in c++ ; and these blocks are glued together in Python. A detail about GNU Radio, its features, the steps that should be followed to install it, etc., is found in [31] or on the main GNU radio page, http://gnuradio.org/trac. Here, only a summary of the most important features is given.

GNU radio has generally the following major features:

Open Source: The code of gnu radio is opensource , so anybody can modify and use it or distribute a new version.

Free: Anybody can use GNU Radio software for free. As a result its correctness is not guaranteed. That means anybody who uses a code of GNU Radio for SDR application uses it at his own risk.

Platform: GNU Radio can work in Linux, UNIX, Mac . GNU Radio can also work in Windows ; despite, the fact that all of the libraries are not yet defined and there are lots of bugs yet to be solved.

Libraries: In addition to base classes which function as building blocks for any radio application; GNU radio contain a set of utility libraries and SDR applications written for different radio applications including spectrum sensing, OFDM transceiver, GSM transceiver, FM receiver, etc.

Data flow Abstraction: This is a nice but difficult to handle feature of Python for other programming language users. Unlike other programming languages; GNU Radio provides data flow abstraction. That is, the data that flows between signal processing blocks can not be accessed.

Programming Language: In GNU Radio signal processing blocks are defined in C++; however, these blocks are glued together and run in Python. This is to make the critical blocks defined in optimized C++ code and to make the connection and management applications in the more user friendly Python language.

Reconfigurable on the fly: Parameters of signal processing blocks can be modified or tuned during run time in GNU Radio.

Flexibility: GNU Radio can be used to form any communication system provided the RF front end is able to perform the high frequency task.

The properties listed above make GNU Radio a suitable software platform for USRP.

B.2 Blocks & Signal Flow Graphs

A signal processing block is an independent module which has input and output ports and a processing gut. In each block, the data received through an input port is stored in a buffer, processed by the signal processing code and then pushed to the output buffer to be sent to the next block. Such an implementation allows a real time operation of signal processing blocks connected together. In addition , each block has its own member functions through which a parameter can be set or be accessed.

A signal flow graph is an interconnection of signal processing blocks that forms a complete radio application. These may for instance be an application which displays the signal level in the environment around a certain carrier frequency. Every signal flow graph starts with a source, uses the required signal processing blocks and ends in a sink. So, when the USRP is used as transmitter it will be set as a sink in a signal flow graph and when it is used as a receiver it will be used as a source in the signal flow graph. Thus, from the application or Python point of view, there is a connection of signal processing blocks between which data flows. Therefore, new blocks to be inserted should be able to be compatible with the already existing blocks.

B.3 Radar Signal Flow Graphs

The radar consist both Tx and Rx, which have its own signal flow graphs.

The radar transmitter consists of :

Signal generator: This section generates modulated symbols. That is, it generates a constant amplitude for CW radar, a pulse for pulse radar and a pseudo random sequence for PRS radar.

Multiplier(gain): After the data is generated, it will be multiplied with a constant corresponding to the transmitter amplitude set by the user.

USRP Sink : Finally the data will be sink to the USRP and the USRP does the transmission task already described.

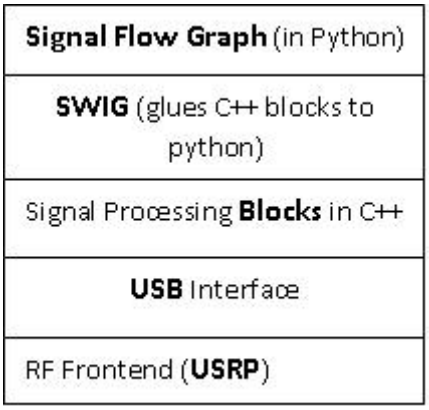

Figure B.1: SDR structure using GNU radio and USRP

So, the transmitter radar flow graph looks like:

$$Signal\,generator \rightarrow Multiplier \rightarrow USRP\,Sink$$

In the radar receiver similarly,

USRP Source: The sampled baseband signal is received by these block.

Data receiver: The received data is correlated with the sent sequence to get impulse response of the channel.

Radar_algorithms: In these blocks the impulse response is processed using the different human movement characterization algorithsms.

Data_sink: The data sink can be a file to store the processed data or it can be a graphical user interface showing the final processed output.

So, the receiver flow graph looks:

$$USRP\,Source \rightarrow Data\,Receiver \rightarrow Radar\,algorithms \rightarrow Data\,Sink$$